Unusual bound states of quark matter within the NJL model

I.N. Mishustin[1,2], **L.M. Satarov**[1,3], **H. Stöcker**[3], **and W. Greiner**[3]

[1] *The Kurchatov Institute, Russian Research Centre, 123182 Moscow, Russia*

[2] *The Niels Bohr Institute, DK–2100 Copenhagen Ø, Denmark*

[3] *Institut für Theoretische Physik, J.W. Goethe Universität, D–60054 Frankfurt am Main, Germany*

Properties of dense quark matter in and out of chemical equilibrium are studied within the SU(3) Nambu–Jona-Lasinio model. In addition to the 4–fermion scalar and vector terms the model includes also the 6–fermion flavour mixing interaction. First we study a novel form of deconfined matter, meso-matter, which is composed of equal number of quarks and antiquarks. It can be thought of as a strongly compressed meson gas where mesons are melted into their elementary constituents, quarks and antiquarks. Strongly bound states in this quark–antiquark matter are predicted for all flavour combinations of $q\overline{q}$ pairs. The maximum binding energy reaches up to 180 MeV per $q\overline{q}$ pair for mixtures with about 70% of strange ($s\bar{s}$) pairs. Equilibrated baryon–rich quark matter with various flavour compositions is also studied. In this case only shallow bound states appear in systems with a significant admixture (about 40%) of strange quarks (strangelets). Their binding energies are quite sensitive to the relative strengths of scalar and vector interactions. The common property of all these bound states is that they appear at high particle densities when the chiral symmetry is nearly restored. Thermal properties of meso-matter as well as chemically equilibrated strange quark matter are also investigated. Possible decay modes of these bound states are discussed.

I. INTRODUCTION

The main goal of present and future experiments with ultrarelativistic heavy ions is to produce and study in the laboratory a new state of strongly interacting matter, the Quark-Gluon Plasma (QGP). In achieving this goal one is facing two major problems. First, the phase structure of QCD is not fully understood yet. Second, the matter evolution in the course of an ultrarelativistic heavy–ion collision may be out of thermodynamical equilibrium.

Most calculations of the QCD phase diagram are made under the assumption of thermal and chemical equilibrium. The QCD lattice calculations at zero baryon chemical potential reveal a second order phase transition or a rapid crossover at temperatures around 140–160 MeV. Recent calculations based on different effective models [1–4] show the possibility of a first order phase transition at finite baryon densities and moderate temperatures. The predicted phase diagram in the $T-\mu$ plane contains a first order transition line terminating at a critical point (T_c, μ_c) with $T_c \simeq 120$ MeV and a finite μ_c [2,3]. Possible signatures of this point in heavy–ion collisions were discussed recently in Ref. [5]. The problem is, however, that the matter produced in central heavy–ion collisions at very high energies has rather low net baryon density. If such a baryon–free matter would expand following (locally) an equilibrium path, it would miss the first order transition line. In this case no clear signatures of the phase transition would be observed.

Moreover, it is most likely that the matter evolution in ultrarelativistic heavy–ion collisions does not follow thermodynamical equilibrium. The reason is that the matter produced in such collisions expands very fast. As has been already observed in heavy–ion experiments at the SPS energies (see e.g. [6]), the expansion velocities along the beam direction are close to the speed of light and the transverse velocities are close to $0.5\,c$. A strong collective expansion of matter is expected also at RHIC and LHC energies. Under such conditions one may expect significant deviations from thermodynamical equilibrium [7], especially from the chemical equilibration. This may happen on both the partonic and the hadronic stages of the reaction.

One can mention at least two mechanisms which may lead to the deviation from chemical equilibrium on the partonic stage. First, it is believed that multiple color strings are produced initially in hard nucleon–nucleon collisions. Later on they decay via the Schwinger mechanism into quark–antiquark pairs whose abundances are determined by quark masses and a string tension constant. At this stage, multiplicities of secondary quarks and antiquarks may be different from their values in thermodynamical equilibrium. Second, simple fits of QCD lattice data [8,9] indicate that gluons may acquire a large effective mass around the deconfinement transition point. Therefore, even if the ideal QGP were created at some intermediate stage of the reaction, gluons would subsequently decay into lighter quark–antiquark pairs. Hence, the abundances of different quark species may deviate strongly from their equilibrium values. In particular, an overpopulation of the light quark–antiquark pairs may be expected. The phase diagram of such a chemically nonequilibrated matter may be very different from the predictions based on the equilibrium concepts.

Another motivation to study chemically nonequilibrated quark–antiquark systems comes from the hadronic spectroscopy. It is well known that some mesonic resonances do not fall into the classification scheme based on the constituent quark model. They cannot be interpreted as conventional $q\overline{q}$ bound states. Rather they could be either bag–like ($qq\bar{q}\bar{q}$) states or meson–meson bound states ($q\bar{q} - q\bar{q}$). Well known examples include the $f_0(980)$ ($K\bar{K}$ bound state close to the threshold), the $f_1(1420)$ ($K\bar{K}^\star$), the $f_0(1500)$ and $f_2(1565)$ ($\omega\omega$ and $\rho\rho$) etc. [10]. A legitimate question is: what will happen if more and more $q\overline{q}$ pairs will be put together? Such multi-$q\overline{q}$ systems might be even more bound due to the reduced surface energy as compared with the bulk one. The mesonic substructure will most likely melt away and such states will look like multi-$q\overline{q}$ bags. We call this hypothetical state of matter as "meso-matter" and its finite droplets at "mesoballs". The analogous state of hadronic matter, bound multipion droplets, has been considered in Ref. [11].

Since the direct application of QCD at moderate temperatures and nonzero chemical potentials is not possible at present, more simple effective models respecting some basic

symmetry properties of QCD are commonly used. One of the most popular models of this kind, which is dealing with constituent quarks and respects chiral symmetry, is the Nambu–Jona-Lasinio (NJL) model [12,13]. In recent years this model has been widely used for describing hadron properties (see reviews [14,15]), phase transitions in dense matter [16–19,2,20] and multiparticle bound states [21–24].

In the previous paper [25] we have used the NJL model to study properties of the quark–antiquark plasma out of chemical equilibrium. In fact, we considered a system with independent densities of quarks and antiquarks. To our surprise, we have found not only first order transitions but also deep bound states even in the baryon–free matter with equal densities of quarks and antiquarks. The consideration in Ref. [25] was limited to systems composed of either light (u, d) or strange (s) quarks and antiquarks. In the present paper we extend the model to arbitrary mixtures of light and strange quarks. The emphasis is put on investigating the possibility of bound states in such systems at various flavour compositions of quarks and antiquarks. As a special case we consider the baryon–rich quark matter in chemical equilibrium, in particular, the possibility of bound states in strange quark matter, i.e. strangelets. Thermal properties of meso-matter and strange quark matter are also studied.

The paper is organized as follows: in Sect. II a generalized NJL model including flavour–mixing terms is formulated in the mean–field approximation. Then in Sect. III the model is used to study the bound states in $q\overline{q}$ systems with different strangeness contents. The model predictions for strangelets are discussed in Sect. IV. The characteristics of bound states at zero temperature are summarized in Sect. V. Effects of finite temperatures are considered in Sect. VI. Possible decay modes of new bound states are discussed in Sect. VII. Main results of the present paper are summarized in Sect. VIII.

II. FORMULATION OF THE MODEL

We proceed from the SU(3)–flavour version of the NJL model suggested in Ref. [26]. The corresponding Lagrangian is written as ($\hbar = c = 1$)

$$\begin{aligned}\mathcal{L} = \overline{\psi}\,(i\,\partial\!\!\!/ - \hat{m}_0)\,\psi + G_S \sum_{j=0}^{8} \left[\left(\overline{\psi}\,\frac{\lambda_j}{2}\,\psi \right)^2 + \left(\overline{\psi}\,\frac{i\gamma_5\lambda_j}{2}\,\psi \right)^2 \right] \\ - G_V \sum_{j=0}^{8} \left[\left(\overline{\psi}\,\gamma_\mu \frac{\lambda_j}{2}\,\psi \right)^2 + \left(\overline{\psi}\,\gamma_\mu \frac{\gamma_5\lambda_j}{2}\,\psi \right)^2 \right] \\ - K \left[\det{}_f \left(\overline{\psi}\,(1-\gamma_5)\,\psi \right) + \det{}_f \left(\overline{\psi}\,(1+\gamma_5)\,\psi \right) \right]. \end{aligned} \tag{1}$$

Here ψ is the column vector consisting of three single–flavour spinors ψ_f, $f = u, d, s$, $\lambda_1, \ldots, \lambda_8$ are the SU(3) Gell-Mann matrices in flavour space, $\lambda_0 \equiv \sqrt{2/3}\,\boldsymbol{I}$, and $\hat{m}_0 = \mathrm{diag}(m_{0u},\, m_{0d},\, m_{0s})$ is the matrix of bare (current) quark masses. At $\hat{m}_0 = 0$ this Lagrangian is invariant with respect to $\mathrm{SU_L}(3) \otimes \mathrm{SU_R}(3)$ chiral transformations. The second and third terms in Eq. (1) correspond, respectively, to the scalar–pseudoscalar and vector–axial-vector 4–fermion interactions. The last 6–fermion interaction term breaks the $U_A(1)$ symmetry and gives rise to the flavour mixing effects. In particular, this term is responsible for the large η' mass [27].

In the mean–field approximation the Lagrangian (1) is reduced to

$$\begin{aligned}\mathcal{L}_{\mathrm{mfa}} = \sum_f \overline{\psi}_f\,(i\not{D} - m_f)\,\psi_f \\ - \frac{G_S}{2}\sum_f \rho_{Sf}^2 + \frac{G_V}{2}\sum_f {\rho_{Vf}}^2 + 4K\prod_f \rho_{Sf}\,, \end{aligned} \tag{2}$$

where $\not{D} = \partial\!\!\!/ + i\,\gamma_0 G_V \rho_{Vf}$ and

$$\rho_{Sf} = <\,\overline{\psi}_f \psi_f\,>\,, \tag{3}$$

$$\rho_{Vf} = <\,\overline{\psi}_f \gamma_0 \psi_f\,> \tag{4}$$

are scalar and vector densities of quarks with flavour f. Angular brackets correspond to the quantum–statistical averaging. The constituent quark masses, m_f, are determined by the coupled set of gap equations

$$m_f = m_{0f} - G_S\,\rho_{Sf} + 2K \prod_{f' \neq f} \rho_{Sf'}\,. \tag{5}$$

The NJL model is non-renormalizable, because its coupling constants have non-trivial dimensions: $G_S,\ G_V \propto [\text{mass}]^{-2}$ and $K \propto [\text{mass}]^{-5}$. As a consequence, the contribution of negative energy states of the Dirac sea are divergent, and one must introduce an ultraviolet cut–off. In this respect the NJL model is an effective model, aimed at describing the non-perturbative regime of QCD at low energies. Following common practice, we introduce the 3–momentum cut–off Λ to regularize divergent integrals. The structure of the fermionic vacuum within the NJL model is shown schematically in Fig. 1(a). Only "active" levels of the Dirac sea, i.e. with $p < \Lambda$ are included in calculations.

The model parameters m_{0f}, G_S, K, Λ can be fixed by reproducing the observed masses of π, K, and η' mesons as well as the pion decay constant f_π. As shown in Ref. [26], a reasonable fit is achieved with the following values:

$$m_{0u} = m_{0d} = 5.5 \text{ MeV}, \quad m_{0s} = 140.7 \text{ MeV}, \tag{6}$$

$$G_S = 20.23 \text{ GeV}^{-2}, \quad K = 155.9 \text{ GeV}^{-5}, \quad \Lambda = 0.6023 \text{ GeV}. \tag{7}$$

Motivated by the discussions in in Refs. [14,28], we choose the following "standard" value of the vector coupling constant[1]

$$G_V = 0.5\,G_S = 10.12\,\text{GeV}^{-2}\,. \tag{8}$$

It should be stressed that the vector and axial–vector terms cannot simply be ignored in the effective Lagrangian (1), as it is often done. These terms are necessary for correctly describing the vector meson properties [27,29], for adjusting the nucleon axial charge g_A [30], etc. In context of the present study, the vector interaction is important, because it generates a net repulsive contribution in asymmetric matter, i.e. when the numbers of quarks and antiquarks are not equal.

---

[1]This value is somewhat different from the one used in our previous paper [25], although the ratio G_V/G_S is the same.

Let us consider homogeneous, thermally (but not, in general, chemically) equilibrated quark–antiquark matter at temperature T. Let $a_{\boldsymbol{p},\lambda}\,(\,b_{\boldsymbol{p},\lambda})$ and $a^+_{\boldsymbol{p},\lambda}\,(\,b^+_{\boldsymbol{p},\lambda})$ be the destruction and creation operators of a quark (an antiquark) in the state $\boldsymbol{p},\lambda$, where $\boldsymbol{p}$ is the 3-momentum and λ is the discrete quantum number denoting spin and flavour (color indices are suppressed). By using the plane wave decomposition of quark spinors in Eq. (2), it can be shown [25] that quark and antiquark phase–space occupation numbers coincide with the Fermi–Dirac distribution functions:

$$< a^+_{\boldsymbol{p},\lambda}\, a_{\boldsymbol{p},\lambda} >\equiv n_{\boldsymbol{p}f} = \left[\exp\left(\frac{E_{\boldsymbol{p}f}-\mu_{Rf}}{T}\right)+1\right]^{-1}, \tag{9}$$

$$< b^+_{\boldsymbol{p},\lambda}\, b_{\boldsymbol{p},\lambda,f} >\equiv \overline{n}_{\boldsymbol{p}f} = \left[\exp\left(\frac{E_{\boldsymbol{p}f}-\overline{\mu}_{Rf}}{T}\right)+1\right]^{-1}, \tag{10}$$

where $E_{\boldsymbol{p}f}=\sqrt{m_f^2+\boldsymbol{p}^2}$ and μ_{Rf}, $\overline{\mu}_{Rf}$ denote the reduced chemical potentials of quarks and antiquarks:

$$\mu_{Rf} = \mu_f - G_V\rho_{Vf}\,, \tag{11}$$

$$\overline{\mu}_{Rf} = \overline{\mu}_f + G_V\rho_{Vf}\,. \tag{12}$$

In our calculations we consider the chemical potentials μ_f and $\overline{\mu}_f$ as independent variables. The assumption of chemical equilibrium with respect to creation and annihilation of $q\overline{q}$ pairs would lead to the conditions

$$\overline{\mu}_f = -\mu_f, \quad f=u,d,s\;. \tag{13}$$

The explicit expression for the vector density can be written as

$$\rho_{Vf} = \rho_f - \overline{\rho}_f\,, \tag{14}$$

where

$$\rho_f = \nu\int\frac{\mathrm{d}^3p}{(2\pi)^3}\,n_{\boldsymbol{p}f}, \quad \overline{\rho}_f = \nu\int\frac{\mathrm{d}^3p}{(2\pi)^3}\,\overline{n}_{\boldsymbol{p}f} \tag{15}$$

are, respectively, the number densities of quarks and antiquarks of flavour f and $\nu=2N_c=6$ is the spin–color degeneracy factor. The net baryon density is obviously defined as

$$\rho_B = \frac{1}{3}\sum_f \rho_{Vf}\,. \tag{16}$$

The physical vacuum ($\rho_f = \overline{\rho}_f = 0$) corresponds to the limit $n_{\boldsymbol{p}f} = \overline{n}_{\boldsymbol{p}f} = 0\,$.

Within the NJL model the energy density and pressure of matter as well as the quark condensates ρ_{Sf} contain divergent terms originating from the negative energy levels of the Dirac sea. As noted above, these terms are regularized by introducing the 3–momentum cutoff $\theta\,(\Lambda - |\boldsymbol{p}|)$, where $\theta\,(x) \equiv \frac{1}{2}\,(1 + \mathrm{sgn}\,x)$. Then the scalar density is expressed as

$$\rho_{Sf} = \nu \int \frac{\mathrm{d}^3 p}{(2\pi)^3} \frac{m_f}{E_{\boldsymbol{p}f}} \left[\, n_{\boldsymbol{p}f} + \overline{n}_{\boldsymbol{p}f} - \theta\,(\Lambda - p)\,\right]. \tag{17}$$

The energy density and pressure are obtained in a standard way from the energy-momentum tensor corresponding to the Lagrangian (2). They can be decomposed into several parts as

$$e = e_K + e_D + e_S + e_V + e_{FM} + e_0\,, \tag{18}$$

$$P = P_K + P_D + P_S + P_V + P_{FM} + P_0\,, \tag{19}$$

These expressions include:

the "kinetic" terms

$$e_K = \nu \sum_f \int \frac{\mathrm{d}^3 p}{(2\pi)^3}\, E_{\boldsymbol{p}f} \left(n_{\boldsymbol{p}f} + \overline{n}_{\boldsymbol{p}f}\right), \tag{20}$$

$$P_K = \frac{\nu}{3} \sum_f \int \frac{\mathrm{d}^3 p}{(2\pi)^3} \frac{\boldsymbol{p}^2}{E_{\boldsymbol{p}f}} \left(n_{\boldsymbol{p}f} + \overline{n}_{\boldsymbol{p}f}\right), \tag{21}$$

the "Dirac sea" terms

$$e_D = -P_D = -\nu \sum_f \int \frac{\mathrm{d}^3 p}{(2\pi)^3}\, E_{\boldsymbol{p}f}\, \theta\,(\Lambda - p), \tag{22}$$

the scalar interaction terms

$$e_S = -P_S = \frac{G_S}{2} \sum_f \rho_{Sf}^2\,, \tag{23}$$

the vector interaction terms

$$e_V = P_V = \frac{G_V}{2} \sum_f \rho_{Vf}^2 \tag{24}$$

and the flavour mixing terms

$$e_{FM} = -P_{FM} = -4K \prod_f \rho_{Sf} \,. \tag{25}$$

A constant $e_0 = -P_0$ is introduced in Eqs. (18) and (19) in order to set the energy density and pressure of the physical vacuum equal to zero. This constant can be expressed through the vacuum values of constituent masses, $m_f^{\rm vac}$, and quark condensates, $\rho_{Sf}^{\rm vac}$. These values are obtained by selfconsistently solving the gap equations (5) in vacuum, i.e. at $n_{\boldsymbol{p}f} = \overline{n}_{\boldsymbol{p}f} = 0$.

For a system with independent chemical potentials for quarks (μ_f) and antiquarks ($\overline{\mu}_f$) one can use the thermodynamic identity

$$e = \sum_f (\mu_f \rho_f + \overline{\mu}_f \overline{\rho}_f) - P + sT \,. \tag{26}$$

Then one can obtain the standard expression for the entropy density,

$$s = \partial_T P_K = -\nu \sum_f \int \frac{{\rm d}^3 p}{(2\pi)^3} \left[n_{\boldsymbol{p}f} \ln n_{\boldsymbol{p}f} + (1 - n_{\boldsymbol{p}f}) \ln (1 - n_{\boldsymbol{p}f}) + n_{\boldsymbol{p}f} \to \overline{n}_{\boldsymbol{p}f} \right] . \tag{27}$$

By using Eqs. (5), (9)–(27) one can also show that the differential relation

$$dP = \sum_f \left(\rho_f \, d\mu_f + \overline{\rho}_f \, d\overline{\mu}_f \right) + s \, dT \tag{28}$$

holds for any thermally (but not necessarily chemically) equilibrated process.

III. SYMMETRIC QUARK–ANTIQUARK MATTER

In this section we study the multi–quark–antiquark systems at zero temperature. Let us consider a symmetric system with equal numbers of quarks and antiquarks for each flavour. This requirement enforces the chemical potentials of quarks and antiquarks to be equal,

$$\overline{\mu}_f = \mu_f \ . \tag{29}$$

In this case the net vector density is automatically zero for each flavour, $\rho_{Vf} = 0$. The net baryon number and electric charge are also zero. Such systems are especially interesting

because the contribution of repulsive vector interaction, Eq. (24), vanishes in this case. One can view such systems as a compressed meson gas where mesons are melted to their elementary constituents, quarks and antiquarks. The single particle states of quarks and antiquarks in such a system are schematically shown in Fig. 1(b). To understand this picture one should simply realize that antiquarks are holes in the Dirac sea. Then one can imagine that a certain number of quarks from the negative energy states are collectively excited into the positive energy states, producing an equal number of holes. Due to the presence of valence quarks and antiquarks the mass gap will be reduced. In this situation one can expect the appearance of bound states.

To characterize the flavour composition we introduce the strangeness fraction parameter

$$r_s = \frac{N_s + N_{\bar{s}}}{N_u + N_{\bar{u}} + N_d + N_{\bar{d}} + N_s + N_{\bar{s}}}\,, \tag{30}$$

where $N_{f(\bar{f})}$ is the number of quarks (antiquarks) of flavour f. For simplicity we consider only the isospin–symmetric mixtures where $N_u = N_d$ and $N_{\bar{u}} = N_{\bar{d}}$.

Fig. 2 shows the energy per particle, $\epsilon = e/\rho_{\rm tot}$, as a function of total density of valence quarks and antiquarks, $\rho_{\rm tot} = \sum\limits_f (\rho_f + \overline{\rho}_f)$, for different r_s. At low densities ϵ tends to the sum of the constituent quark and antiquark masses in vacuum, weighted according to r_s,

$$\epsilon(\rho_{\rm tot} \to 0, r_s) = m_q^{\rm vac}(r_s) = (1 - r_s)\, m_u^{\rm vac} + r_s\, m_s^{\rm vac}. \tag{31}$$

With growing density, ϵ first decreases due to the attractive scalar interaction. At higher densities ϵ starts to increase, approaching slowly the limit of ideal ultrarelativistic Fermi gas. For each r_s one can see the appearance of a nontrivial minimum corresponding to a bound multiparticle state with $\epsilon_{\rm min}\,(r_s) < m_q^{\rm vac}(r_s)$. The density of $q\overline{q}$ pairs in these bound states varies between 0.7 and 1.4 fm^{-3}, depending on r_s. It is easy to see [25] that the minimum in ϵ at any r_s corresponds to zero pressure. Thus, finite droplets of such matter could be in mechanical equilibrium with vacuum.

A more detailed behaviour of ϵ in the plane $\rho_{u+d} - \rho_s$ is shown in Fig. 3(a) (here $\rho_{u+d} = \rho_u + \rho_d = 2\,\rho_u$). The condition of fixed r_s corresponds to a straight line with slope

$r_s/(1-r_s)$ starting from the origin. By inspecting the figure one can notice the valley of local minima[2] starting from $\epsilon = 0.482$ GeV per particle in the pure $s\bar{s}$ system ($r_s = 1$) and descending to $\epsilon = 0.304$ GeV per particle in pure $u\bar{u} + d\bar{d}$ matter ($r_s = 0$). There is no potential barrier on the way from $r_s = 1$ to $r_s = 0$. Thus, a droplet with any $r_s \neq 0$ will eventually "roll down" in the state with $r_s = 0$. Possible decay modes of the considered bound states are discussed in Sect. VII.

The constituent masses of u and s quarks as functions of ρ_{tot} are shown in Fig. 4 for different r_s. As expected, the constituent masses decrease with density, signaling the gradual restoration of chiral symmetry. It is interesting to note that the constituent mass m_f is more sensitive to the density of the same flavour f. For instance, in pure $u\bar{u} + d\bar{d}$ matter, i.e. at $r_s = 0$, the s-quark mass does not change much with density. In this case m_s varies entirely due to the flavour–mixing interaction. At densities corresponding to the bound states (indicated by dots on the respective curves) the constituent masses drop significantly as compared to their vacuum values: $m_{u,d} \simeq 0.1\, m_{u,d}^{\rm vac}\,, m_s \simeq 0.3\, m_s^{\rm vac}$. For zero bare masses, $m_{0f} = 0$, the constituent quark masses in bound states would be practically zero. This means that the bound states correspond to the Wigner phase where chiral symmetry is restored.

Fig. 5 shows the chiral condensate $\langle \bar{u}u \rangle$ which, in our notation (see Eq. (3)), coincides with the scalar density ρ_{Su} (notice the minus sign on the vertical axis). Its behaviour is strongly correlated with the u–quark constituent mass (compare with Fig. 4). As before, the variation of the $\langle \bar{u}u \rangle$ condensate is mainly sensitive to the density of valence u–quarks and antiquarks. At $r_s = 1$, when this density is zero, the change in the $\bar{u}u$ condensate is caused by the flavour–mixing interaction. The behaviour of the $\langle \bar{s}s \rangle$ condensate is qualitatively similar, but due to the larger bare mass, $m_{0s} \simeq 140$ MeV, its density dependence is weaker.

The u and s chemical potentials are shown in Fig. 6. It is interesting that initially they

[2]This valley is shown by the dotted line in Fig. 3(a).

drop and then rise with density. One can easily understand this behaviour by analyzing the explicit expression for μ_f,

$$\mu_f = \sqrt{m_f^2 + p_{Ff}^2}\ , \tag{32}$$

where $p_{Ff} = (6\pi^2\rho_f/\nu)^{1/3}$ is the Fermi momentum of quarks with flavour f (antiquarks have the same Fermi momentum in symmetric matter). At low densities, when $p_{Ff} \ll m_f$ and $\mu_f \simeq m_f$, all chemical potentials decrease with density together with the respective constituent mass m_f (see Fig. 4). At high densities, when $p_{Ff} \gg m_f$, the chemical potential grows with density as in the free relativistic Fermi–gas, $\mu_f \simeq p_{Ff} \propto \rho_f^{1/3}$. In fact, this nontrivial behaviour of μ_f is responsible for the first order phase transition discussed below.

IV. STRANGE QUARK MATTER

Let us turn now to quark matter with nonzero net baryon density at $T = 0$. We assume that only valence quarks are present, i.e. the density of valence antiquarks is zero for each flavour ($\overline{\rho}_f = 0$). In other words, this means that all levels in the Dirac sea are filled up, and additionally some levels in the Fermi sea are occupied by the valence quarks. This situation is schematically shown in Fig. 1(c). In contrast to the symmetric $q\overline{q}$ matter discussed above, now the symmetry between positive and negative energy states is lost due to the presence of repulsive vector interaction.

Fig. 7 shows the energy per baryon ϵ as a function of baryon density, $\rho_B = \frac{1}{3}\sum_f \rho_f$. Different curves correspond to different r_s, which in this case is simply the ratio of the strange quark density to the total density of all quarks. At $\rho_B \to 0$ the energy per quark tends to the corresponding vacuum mass given by Eq. (31). With growing density both the attractive scalar and repulsive vector interactions contribute to ϵ. It is interesting that at $r_s \leq 0.7$ the attractive interaction is strong enough to produce a nontrivial local minimum at a finite ρ_B. In the pure u, d matter ($r_s = 0$) this minimum is unbound by about 20 MeV as compared to the vacuum masses of u and d quarks. On the other hand, it is located at a

baryon density of about $1.8\,\rho_0$, which is surprisingly close to the saturation density of normal nuclear matter. Of course, the location of this minimum depends on the model parameters. Nevertheless, one can speculate that nucleon–like 3–quark correlations, not considered in the mean–field approach, will turn this state into the correct nuclear ground state.

When r_s grows from 0 to about 0.4, the local minimum is getting more pronounced and the corresponding baryon density increases to about $3.2\,\rho_0$. At larger r_s, the minimum again becomes more shallow and disappears completely at $r_s \simeq 0.7$. At $0.2 < r_s < 0.6$ the minima correspond to the true bound states, i.e. the energy per quark is lower than the respective vacuum mass. But in all cases these bound states are rather shallow: even the most strongly bound state at $r_s \simeq 0.4$ is bound only by about 5 MeV per quark or 15 MeV per baryon. Nevertheless, the appearance of local minima signifies the possibility for finite droplets to be in mechanical equilibrium with the vacuum at $P = 0$. It is natural to identify such droplets with strangelets, which are hypothetical objects made of light and strange quarks [31–36]. Similar multiparticle bound states made of nucleons and hyperons were also discussed [37–39].

It should be emphasized here that β–equilibrium is not required in the present approach (see the discussion below). That is why our most bound strangelets are predicted to be more rich in strange quarks ($r_s > 1/3$) than in the approaches assuming β–equilibrium [31,32,34], which give $r_s < 1/3$. As a result, these strangelets will be negatively charged[3]. Indeed, the ratio of the charge Q to the baryon number B is expressed through r_s as

$$\frac{Q}{B} = \frac{2}{3}\frac{\rho_u}{\rho_B} - \frac{1}{3}\frac{\rho_d}{\rho_B} - \frac{1}{3}\frac{\rho_s}{\rho_B} = \frac{1}{2}(1 - 3r_s). \tag{33}$$

For $r_s \simeq 0.4$ this gives $Q/B \simeq -0.1$. In light of recent discussions (see e.g. Ref. [36]) concerning possible dangerous scenarios of the negatively–charged strangelet production at RHIC, we should emphasize that the strangelets predicted here are not absolutely bound[4],

[3]Negatively–charged strangelets have been also considered in Refs. [33,35].

[4]The analogous conclusion has been made in Ref. [24].

i.e. their energy per baryon is higher than that for the normal nuclear matter. Hence, the spontaneous conversion of normal nuclear matter to strange quark matter is energetically not possible.

The behaviour of the energy per quark for arbitrary mixtures of light and strange quarks is shown in Fig. 3(b). One can clearly see that the valley corresponding to the local minima has always a positive slope in r_s. There is no potential barrier separating the states with $r_s \neq 0$ and $r_s = 0$. Thus, a strangelet with any $r_s \neq 0$ will freely roll down to the normal nuclear matter state with $r_s = 0$. It is interesting to note that a barrier in r_s may appear if attractive scalar interaction is arbitrarily enhanced in the strange sector [35].

Fig. 8 shows the constituent masses of u and s quarks as functions of baryon density. The dropping masses manifest again a clear tendency to the restoration of chiral symmetry at high densities. As before, the dots indicate the masses at the local minima in the respective energies per baryon shown in Fig. 7. These mass values are somewhat larger than in the symmetric $q\overline{q}$ matter discussed above (see Fig. 4). Note that the stronger is reduction of constituent masses the deeper are the corresponding bound states. For the metastable state at $r_s = 0$, which is a candidate for the nuclear ground state, the masses of u and s quarks are equal to 0.3 and 0.9 of their vacuum values respectively. For the most bound state at $r_s \simeq 0.4$ the respective mass ratios are reduced to 0.15 and 0.6.

The behaviour of the u and s chemical potentials is shown in Fig. 9. One can notice the differences as compared with symmetric $q\overline{q}$ matter (Fig. 6). In particular, the curves for different r_s do not intersect. Due to the additional contribution of the vector interaction, which is linear in ρ_B (see Eq. (11) where $\mu_{Rf} = \sqrt{m_f^2 + p_{Ff}^2}$ at $T = 0$), the minima in μ_u and μ_s are less pronounced. At $r_s > 0.7$ the curves have no minima at all. Therefore the chiral phase transition will be not as strong in this case as in symmetric matter.

V. SYSTEMATICS OF BOUND STATES

The properties of the multiparticle bound states discussed in preceding sections are summarized in Figs. 10–11. Fig. 10 shows the binding energy per quark, $m_q^{\rm vac}(r_s) - \epsilon_{\rm min}(r_s)$, where $m_q^{\rm vac}$ is the energy at $\rho_{tot} = 0$ and $\epsilon_{\rm min}(r_s)$ is the energy at a local minimum, both taken for a given r_s value. To avoid misunderstanding, Figs. 11(a) and 11(b) show $\epsilon_{\rm min}(r_s)$ separately. Although the absolute minimum of $\epsilon_{\rm min}$ corresponds to $r_s = 0$, the maximum bindings are realized at nonzero r_s. For symmetric $\bar{q}q$ systems the maximum value of about 90 MeV is reached for $r_s \simeq 0.7$. This is indeed very strange and very bound matter! For asymmetric systems, where $\overline{\rho}_f = 0$, the maximum binding energy is much smaller, about 5 MeV per quark at $r_s \simeq 0.4$. One should bear in mind, however, that in this case $\epsilon_{\rm min}$ results from a strong cancellation between the attractive scalar and repulsive vector interactions. Therefore, it is very sensitive to their relative strengths. The results presented above are obtained for $G_V = 0.5\, G_S$. For comparison in Figs. 10 and 11(b) we also present the model predictions for $G_V = 0$. In this case the maximum binding energy increases to about 30 MeV per quark and the corresponding r_s value shifts to about 0.6. It is interesting to note that for $G_V = 0$ the bound state appears even in the pure u, d matter. The corresponding binding energy is about 7 MeV per quark, i.e. 21 MeV per baryon.

Figures 10 and 11 reveal some differences compared to the previous calculations in Ref. [25]. This is mainly due to a different set of model parameters used there. In particular, the present set of parameters gives higher quark constituent masses in the vacuum, $m_{u,d}^{\rm vac} \simeq 368$ MeV and $m_s^{\rm vac} \simeq 550$ MeV, as compared to $m_{u,d}^{\rm vac} = 300$ MeV and $m_s^{\rm vac} = 520$ MeV in Ref. [25]. This leads to an overall upward shift in the energy per particle by 30–60 MeV. On the other hand, inclusion of the flavour–mixing interaction lowers the energy. As a result, all binding energies increase slightly. A local minimum in ϵ appears now even in the pure u, d matter.

The dots in Fig. 11 indicate the positions of some conventional mesons (a) and baryons (b). Their empirical masses are rescaled (by factor 1/2 for mesons and 1/3 for

baryons) and shown at r_s values corresponding to their flavour compositions. By inspecting the figure, one can make a few interesting observations. According to Fig. 11(a), mesoballs lie lower in energy than conventional vector mesons, but higher than the pseudoscalar mesons (see discussion in Sect. VIII). As one can see in Fig. 11(b), conventional baryons are more bound than strangelets even at $G_V = 0$. This is an indication that baryon–like 3–quark correlations might be indeed very important in the baryon–rich quark matter.

VI. QUARK MATTER AT FINITE TEMPERATURES

In this section we study properties of deconfined matter at finite temperatures. The calculations for this case can be done by using general formulas of Sect. II with the quark and antiquark occupation numbers given by Eqs. (9)–(10).

First we discuss thermal properties of meso-matter where the chemical potentials obey the conditions (29). A typical behaviour of the equation of state for this case is illustrated in Fig. 12(a). It shows the pressure isotherms for symmetric $q\bar{q}$ matter with strangeness content $r_s = 1/3$. One can clearly see a strong first order phase transition which is signaled by the appearance of isotherms with negative slopes, $\partial_\rho P < 0$ (spinodal instability). The corresponding critical temperature is about 100 MeV. Another important feature is that the zero-pressure states persist up to temperatures as high as 70 MeV. This means that a finite droplet of this matter which has cooled down to this temperature and still remaining at high density of $q\bar{q}$ pairs (around $4\,\rho_0$ in this case), will be trapped in a bound state. At later times it will further cool down by emitting hadrons from the surface (see below).

The critical temperatures for a phase transition and for the appearance of a bound state are shown in Fig. 13(a) as functions of r_s. One can conclude that this dependence is rather weak: the first critical temperature changes between 90 and 110 MeV while the second one varies around 70 MeV.

Now let us consider chemically–equilibrated quark matter at finite temperatures. In this case the chemical potentials of quarks obey the conditions (13). Fig. 12(b) represents the

pressure isotherms for the case $\mu_s = 0$. This condition implies equal numbers of strange quarks and antiquarks, i.e. zero net strangeness. It is appropriate for fast processes where strangeness is conserved, e.g. in relativistic nuclear collisions. As before one can see a region of spinodal instability, $\partial_\rho P < 0$, which is characteristic for a first order phase transition. However, this phase transition is much weaker than in the case of symmetric $q\bar{q}$ matter (note the different scales in Figs. 12(a) and 12(b)). The corresponding critical temperature is about 35 MeV in this case. The zero–pressure states exist only at temperatures below 15 MeV.

Generally, the equation of state of the chemically equilibrated quark matter is characterized by two quantities: net baryon charge, B, and net strangeness, S. Therefore, it is interesting to study thermal properties of this matter at $S \neq 0$. Such states can be reached in neutron stars. They can also be realized via the distillation mechanism accompanying a QCD phase transition in heavy–ion collisions [40]. Leaving a detailed study of this question for a future publication, here we only present results which complement our discussion concerning Fig. 13(a). Fig. 13(b) shows the critical temperatures for the phase transition and for the bound states in the equilibrated matter as functions of $r_s^- = S/3B$ [5]. One can see that both temperatures first grow with r_s^- and then drop to zero at $r_s^- \sim 0.8$. The maximal values of respectively 50 MeV and 30 MeV are realized at some intermediate r_s^- around 0.4. As demonstrated earlier in Fig. 10, this value of r_s^- corresponds to the most bound state of strange quark matter at $T = 0$. So we see an obvious correlation: the deeper is a bound state at $T = 0$ the stronger is a phase transition at finite temperatures.

It should be emphasized here again that the thermal properties of asymmetric baryon–rich quark matter are very sensitive to the relative strength of scalar and vector interactions. To illustrate this point we have calculated the phase diagrams for several values of G_V.

---

[5] We introduce this new notation in order to distinguish this quantity from r_s defined in Eq. (30). In chemically equilibrated matter at $T = 0$ (no antiquarks) these two quantities coincide.

The results for $\mu_s = 0$ are presented in Fig. 14. It shows the boundaries of two–phase coexistence regions calculated by using standard Gibbs conditions [25]. If we take $G_V = 0$, as in most calculations in the literature, the coexistence region becomes wider and the corresponding critical temperature increases to about 70 MeV. On the other hand, if one takes $G_V = 0.65\, G_S$, the phase transition becomes weaker: the critical temperature moves down to 20 MeV and the zero–pressure states disappear completely. The calculation shows that there is no phase transition at $G_V > 0.71\, G_S$. It is interesting to note that in all cases this first order phase transition occupies the region of densities around the normal nuclear density ρ_0. For instance, at $G_V = 0.5\, G_S$ the coexistence region at $T = 0$ extends from 0.2 to 1.7 ρ_0.

These results demonstrate that this chiral phase transition is rather similar to a liquid–gas phase transition in normal nuclear matter. The critical temperature and baryon density in the present case ($T_c \sim 30$ MeV, $\rho_{Bc} \sim \rho_0$) are not so far from the values predicted by the conventional nuclear models [41] ($T_c \sim 20$ MeV, $\rho_{Bc} \sim 0.5\, \rho_0$). One may expect that in a more realistic approach, taking into account nucleonic correlations, the "chiral" transition may turn into the ordinary "liquid–gas" phase transition. If this would be the case, one should be doubtful about the possibility of any other QCD phase transition of the liquid–gas type at a higher baryon density. At least only one phase transition of this type is predicted within the NJL model.

VII. DISCUSSION OF DECAY MODES

Let us discuss briefly possible decay channels of the novel states of quark matter described above. Naively one could think that the symmetric $q\overline{q}$ matter would be extremely unstable with respect to the annihilation of quarks and antiquarks. But, in fact, many annihilation channels are closed or do not exist in dense $q\overline{q}$ matter. From the first sight, one may think that two–pion annihilation, $\bar{q} + q \to \pi + \pi$, should be the strongest decay channel in the bulk (one–pion annihilation is not allowed by the energy–momentum conservation). But

simple arguments show that this might be not true. Indeed, the bound states of $q\overline{q}$ matter appear at such high densities when chiral symmetry is practically restored. In this case the pion looses its special nature as a Goldstone boson and inside this matter it should be as heavy as other mesons. Moreover, due to the Mott transition [42], it is unlikely that conventional mesonic states survive in this dense medium. Therefore, one can expect that the hadronic channels of the $q\overline{q}$ annihilation simply do not exist in the bulk.

Another possible decay channel is the strong flavour conversion, $\bar{s}s \to \bar{u}u$ or $\bar{d}d$. In principle, this process can proceed through the one–gluon (color octet) intermediate state. However, it may be shown that due to color neutrality the corresponding matrix elements vanish after summation over the color indices. Within the present approach, the 4–fermion interaction terms are diagonal in the flavour space (see Eq. (2)) and, therefore, cannot change the flavour. Strong flavour conversion is possible only through the 6–fermion flavour–mixing interaction, $\bar{s}s \to \bar{u}u + \bar{d}d$. This channel is only open when $\mu_s > \mu_u + \mu_d$. By inspecting Fig. 6 one can see that this condition is never fulfilled. Therefore we conclude that strong flavour conversion is not possible or at least strongly suppressed in the bulk.

In a finite droplet, hadronic annihilation, $\bar{q_f} + q_{f'} \to h_1 + h_2 + ...$, is certainly possible at the surface, if $\bar{\mu}_f + \mu_{f'} > m_{h_1} + m_{h_2} + ...$. It is clear from Fig. 11(a) that the emission of pions in annihilation of light $q\overline{q}$ pairs is energetically more favorable than the emission of heavier mesons. Moreover, many annihilation channels of strange quarks and antiquarks are simply closed e.g. $\overline{s} + s \to K + \overline{K}$. As a result of the pion emission, the strangeness content of the daughter droplet will increase[6]. Finally, it will contain predominantly the $s\bar{s}$ pairs, similarly to a system composed of ϕ–mesons ("ϕ–ball").

Further hadronization may be slowed down by several reasons [25]. According to Fig. 10, at $r_s \simeq 1$ the energy available in the annihilation of a $s\bar{s}$ pair is $\mu_s + \bar{\mu}_s \simeq 0.95$ GeV. This is lower than the threshold energies of the hadronic states $\phi(1020)$ and $K\bar{K}(990)$. The only

[6]Similar processes leading to strangeness distillation have been considered in Refs. [33,40].

open channels in this case are $\rho\pi(910)$ and $3\pi(420)$. Their partial width in the ϕ-meson decay is about 0.7 MeV. If this would be the dominant decay mode, one could expect a life time for these ϕ–balls of about 280 fm/c, i.e much longer than the typical duration of a heavy–ion collision.

In strange quark matter (without antiquarks), flavour conversion is only possible through weak decays. As follows from Fig. 9, at densities corresponding to zero pressure, the condition $\mu_s > \mu_u$ holds. This means that weak processes of the types $s \to u + e^- + \overline{\nu}_e$, $s + u \to u + d$ are allowed. Since there is no local barrier at any r_s (see Fig. 11(b)), a system produced initially at some $r_s \neq 0$ will subsequently reduce this r_s value by a cascade of weak decays. As a result, the system will roll down along the line of local minima shown in Fig. 11(b) (see also Fig. 3(b)). Finally, all s quarks will be converted into light u, d quarks. Two steps of this conversion process are shown schematically in Figs. 15(a) and 15(b).

This picture is very different as compared to the one based on the MIT bag model. Within that model the pressure and energy density are given by simple expressions

$$P_{\rm MIT} = P_{\rm id} - B, \quad e_{\rm MIT} = e_{\rm id} + B \ , \tag{34}$$

where B is a bag constant, $P_{\rm id}$ and $e_{\rm id}$ are the pressure and energy density for a mixture of ideal gases of u, d and s quarks with constant (bare) masses, $m_{u,d} = m_{0u,d} \simeq 0$, $m_s = m_{0s} \simeq 150$ MeV. By properly choosing B one can always get a zero pressure point and, accordingly, a minimum in the energy per baryon. Because the quark masses are kept constant, the condition $\mu_s > m_s$ will be first satisfied at a relatively low baryon density $\propto m_{0s}^3$. At higher densities a certain fraction of s quarks will always be present in a β–equilibrated matter.

In contrast, in the NJL model the s quark mass is a function of both baryon density and strangeness content. As one can see from Fig. 9, at any given r_s the condition $\mu_{u,d} = \mu_s$ can be satisfied only at sufficiently high baryon densities which correspond to positive pressure. On the other hand, at the points of zero pressure we always have $\mu_{u,d} < \mu_s$. Therefore, weak

decays will proceed until a strangelet reaches $r_s = 0$ (see Fig. 15(c)).

VIII. CONCLUSIONS

In the present paper we have investigated properties of deconfined matter at different densities of quarks and antiquarks, not necessarily constrained by the conditions of chemical equilibrium. All calculations are carried out within the SU(3)–flavour NJL model including scalar, vector and flavour–mixing interactions. We have demonstrated the possibility of strongly bound states in symmetric $q\overline{q}$ systems consisting of equal numbers of quarks and antiquarks ("mesoballs"). The maximal binding energies of mesoballs, of about 90 MeV per particle or 180 MeV per $q\overline{q}$ pair, are realized for flavour compositions with about 70% of $s\overline{s}$ pairs. These systems remain bound up to the temperatures $T \lesssim 70\,\mathrm{MeV}$. The lifetimes of mesoballs may be long enough due to the suppression of annihilation into hadrons in the bulk. The model predicts a strong first order phase transition in chemically nonequilibrated meso-matter, i.e. at zero net baryon density. The critical temperature of this phase transition is in the range of 90–110 MeV depending of the relative abundance of $s\overline{s}$ pairs. As discussed in Ref. [25], formation of mesoballs in high–energy heavy–ion collisions may be observed through the event–by–event analysis of π, K, ϕ spectra. In particular, narrow bumps in the hadron rapidity distributions may be generated by hadronizing mesoballs.

By using the same model, we have also investigated the equation of state of chemically equilibrated deconfined matter at various temperatures, baryon densities and strangeness contents. The model predicts the existence of loosely bound, negatively–charged strangelets with maximal binding energies of about 20 MeV per baryon at $r_s \sim 0.4$. Similarly to Ref. [24], no absolutely stable strange quark matter has been found. It is shown that properties of baryon–rich quark matter are very sensitive to the relative magnitude of the vector and scalar interactions. At the standard value of vector and scalar couplings, $G_V/G_S = 0.5$, the metastable bound states of chemically equilibrated matter exist at $T < 15$ MeV, while at $G_V = 0$ this temperature increases to 40 MeV.

The first order chiral phase transition in equilibrated baryon–rich quark matter is much weaker as compared to the symmetric $q\bar{q}$ matter. In the case of zero net strangeness the critical temperature is in the range of 30 MeV and the critical baryon density is around ρ_0. We believe that this phase transition is reminiscent of the ordinary liquid–gas phase transition in nuclear matter. One can use the present model to study the chiral phase transition at nonzero net strangeness, which is appropriate e.g. for neutron star matter. We have found that the maximal critical temperature $T_c \simeq 50$ MeV is reached for the ratio of net strangeness to baryon charge $S/B \simeq 1.2$.

It should be emphasized that all calculations in this paper have been made with constant values of coupling constants G_S, G_V, K . We think that, this is a reasonable approximation at intermediate densities and temperatures. On the other hand, the asymptotic freedom of QCD requires all effective interactions to vanish at high densities and temperatures. Therefore, in a more realistic approach the coupling constants should decrease with density and temperature. Hopefully, this behaviour can be simulated by introducing finite range form factors.

ACKNOWLEDGMENTS

The authors thank M. Belkacem and J. Schaffner-Bielich for useful discussions. Two of us (I.N.M. and L.M.S.) thank the Institut für Theoretische Physik, J.W. Goethe Universität, Frankfurt am Main, for the kind hospitality. This work has been supported by the Alexander von Humboldt Stiftung, the Graduiertenkolleg "Experimentelle und Theoretische Schwerionenphysik", GSI, BMBF and DFG.

---

[1] L.P. Csernai, I.N. Mishustin, and A. Mocsy, Heay Ion Physics **3**, 151 (1996);

A. Mocsy, M.Sc. thesis, University of Bergen, 1996.

[2] J. Berges and K. Rajagopal, Nucl. Phys. **B538**, 215 (1999).

[3] M.A. Halasz, A.D. Jackson, R.E. Shrock, M.A. Stephanov, and J.J.M. Verbaarshot, Phys. Rev. D **58**, 096007 (1998).

[4] G.W. Carter, D. Diakonov, Nucl. Phys. **A642**, 78 (1998).

[5] M. Stephanov, K. Rajagopal, E. Shuryak, Phys. Rev. Lett. **81**, 4816 (1998).

[6] P. Braun–Munzinger and J. Stachel, Nucl. Phys. **A638**, 3c (1998).

[7] I.N. Mishustin, Phys. Rev. Let. **82**, 4779 (1999).

[8] P. Levai, U. Heinz, Phys. Rev. C **57**, 1879 (1998).

[9] G.W. Carter, O. Scavenius, I.N. Mishustin, and P.J. Ellis, nucl-th/9812014.

[10] Particle Data Group. C. Caso et. al., Eur. Phys. J. **3**, 1 (1998).

[11] I.N. Mishustin and W.Greiner, J. Phys. **G19**, L101 (1993).

[12] Y. Nambu and G. Jona-Lasinio, Phys. Rev. **122**, 345 (1961); **124**, 246 (1961).

[13] V.G. Vaks and A.I. Larkin, Sov. J. JETP **13**, 192 (1961).

[14] U. Vogl and W. Weise, Prog. Part. Nucl. Phys. **27**, 195 (1991).

[15] S.P. Klevansky, Rev. Mod. Phys. **64**, 649 (1992).

[16] M. Asakawa and Y. Yazaki, Nucl. Phys. **A504**, 668 (1989).

[17] S. Klimt, M. Lutz, and W. Weise, Phys. Lett. **B249**, 386 (1990).

[18] J. Cugnon, M. Jaminon, and B. Van den Bossche, Nucl. Phys. **A598**, 515 (1996).

[19] K.G. Klimenko and A.S. Vshivtsev, Zh. Eksp. Teor. Fiz. **84**, 1047 (1997) [Sov. J. JETP **84**, 1057 (1997)] ;

D. Ebert, K.G. Klimenko, M.A. Vdovichenko, and A.S. Vshivtsev, Phys. Rev. D **61**, 025005 (2000).

[20] T.M. Schwarz, S.P. Klevansky, and G. Rapp, Phys. Rev. C **60**, 055205 (1999).

[21] V. Koch, T.S. Biro, J. Kunz, and U. Mosel, Phys. Lett. **B185**, 1 (1987);
V. Koch, B. Blättel, and U. Mosel, *ibid.* **B194**, 331 (1987).

[22] M. Buballa, Nucl. Phys. **A611**, 393 (1996);
M. Buballa and M. Oertel, *ibid.* **A642**, 39 (1998).

[23] I.N. Mishustin, in Proc. Int. Conf. *Nuclear Physics at the Turn of the Millenium* (Wilderness, South Africa, 1996), eds. H. Stöcker, A. Gallman, and J.H. Hamilton, World Scientific, 1997, p. 522.

[24] M. Buballa and M. Oertel, Phys. Lett. **B457**, 261 (1999).

[25] I.N. Mishustin, L.M. Satarov, H. Stöcker, and W. Greiner, Phys. Rev. C **59**, 3343 (1999).

[26] P. Rehberg, S.P. Klevansky, and J. Hüfner, Phys. Rev. C **53**, 410 (1996).

[27] S. Klimt, M. Lutz, U. Vogt, and W. Weise, Nucl. Phys. **A516**, 429 (1990).

[28] W. Ehehalt and W. Cassing, Nucl. Phys. **A602**, 449 (1996).

[29] A. Polleri, R.A. Broglia, P.M. Pizzochero, and N.N. Scoccola, Z. Phys. **A357**, 325 (1997).

[30] M. Lutz, S. Klimt, and W. Weise, Nucl. Phys. **A542**, 521 (1992).

[31] E. Witten, Phys. Rev. D **30**, 292 (1984).

[32] E. Farhi and R.L. Jaffe, *ibid.* **30**, 2379 (1984).

[33] C. Greiner, P. Koch, and H. Stöcker, Phys. Rev. Lett. **58**, 1825 (1987).

[34] E.P. Gilson and R.L. Jaffe, Phys. Rev. Lett. **71**, 332 (1993).

[35] J. Schaffner-Bielich, Nucl. Phys. **A639**, 443 (1998).

[36] W. Busza, R.L. Jaffe, J. Sandweiss, and F. Wilczek, hep-ph/9910333.

[37] M. Rufa, J. Schaffner, J. Maruhn, H. Stćker, and W. Greiner, Phys. Rev. C **42**, 2469 (1990).

[38] J. Schaffner, C.B. Dover, A. Gal, C. Greiner, and H. Stöcker, Phys. Rev. Lett. **71**, 35 (1993).

[39] J. Schaffner, C.B. Dover, A. Gal, C. Greiner, D.J. Millener, and H. Stöcker, Ann. Phys. (N.Y.) **235**, 35 (1994).

[40] C. Greiner and H. Stöcker, Phys. Rev. D **44**, 3517 (1991).

[41] A.I. Goodman, J.I. Kapusta, and A.Z. Mekjian, Phys. Rev. C **30**, 851 (1984).

[42] P. Zhuang, J. Hüfner, and S.P. Klevansky, Nucl. Phys. **A576**, 525 (1994).

FIGURE CAPTIONS

FIG. 1. Schematic picture of energy levels of quarks and antiquarks in vacuum (a), symmetric $q\overline{q}$ droplet (b) and pure quark droplet (c). Occupied quark states are shown by full dots while open dots represent holes (antiquarks). R denotes the radius of a droplet, m and V are, respectively, constituent mass and vector potential of quarks. The boundaries of vacuum mass gap are shown by dashed lines.

FIG. 2. Energy per particle ϵ in symmetric $q\overline{q}$ matter vs. total particle density at different values of strangeness fraction r_s (shown near the corresponding curves). Points indicate local minima of ϵ. $\rho_0 = 0.17\,\mathrm{fm}^{-3}$ is normal nuclear density.

FIG. 3. Contours of energy per particle ϵ (in GeV) for symmetric (a) and asymmetric (b) matter in the $\rho_{u+d} - \rho_s$ plane. Dotted lines represent local extrema of ϵ. Shading shows regions with negative pressure.

FIG. 4. Constituent masses of u and s quarks in symmetric $q\overline{q}$ matter as functions of total particle density. Figures in the box show values of strangeness fraction r_s. Dots correspond to minima of energy per particle at given r_s.

FIG. 5. The same as in Fig. 4, but for condensate densities of u and s quarks.

FIG. 6. The same as in Fig. 4, but for chemical potentials of u and s quarks.

FIG. 7. The same as in Fig. 2, but for asymmetric u, d, s matter without antiquarks.

FIG. 8. The same as in Fig. 4, but for asymmetric quark matter.

FIG. 9. The same as in Fig. 6, but for asymmetric quark matter.

FIG. 10. Binding energies per particle in symmetric $q\overline{q}$ matter (solid line) and asymmetric quark matter as functions of strangeness fraction r_s. Dotted line shows the results of calculations when the vector interaction is switched off ($G_V = 0$).

FIG. 11. Minimal energies per particle in symmetric (a) and asymmetric (b) matter as functions of strangeness fraction r_s. Dotted lines show energy per particle in the limit of zero particle densities, Eq. (31). Different parts of the solid line in the lower panel correspond to metastable (AB and CD) or bound (BC) states. Triangles and squares show masses of lightest mesons and baryons devided by the total number of constituents (two in mesons and three in baryons). Symbol $< K >$ represents the spin averaged mass of K and $K^*(892)$ mesons, i.e. $(3m_{K^*} + m_K)/8$. Dashed line in the lower plot shows the results in the limit $G_V \to 0$.

FIG. 12. Pressure isotherms for symmetric $q\overline{q}$ matter (a) and equilibrated quark matter with $\mu_s = 0$ (b). Temperatures are given in MeV near the corresponding curves. Boundaries of spinodal regions are shown by the dashed lines.

FIG. 13. Critical temperatures for existence of bound states ($P < 0$) and phase transition ($\partial_\rho P < 0$) in symmetric $q\overline{q}$ matter (a) and equilibrium quark matter (b) as functions of strangeness fraction.

FIG. 14. Phase diagrams of equilibrium quark matter with zero net strangeness at various ratios of vector and scalar coupling constants.

FIG. 15. Schematic pictures of energy levels (shown by shading) occupied by light and strange quarks in cold quark matter at different strangeness fractions r_s. Hatched boxes represent the constituent quark masses. Arrows show weak decay processes $s \to u + e + \overline{\nu}_e$ and $s + u \to u + d$.

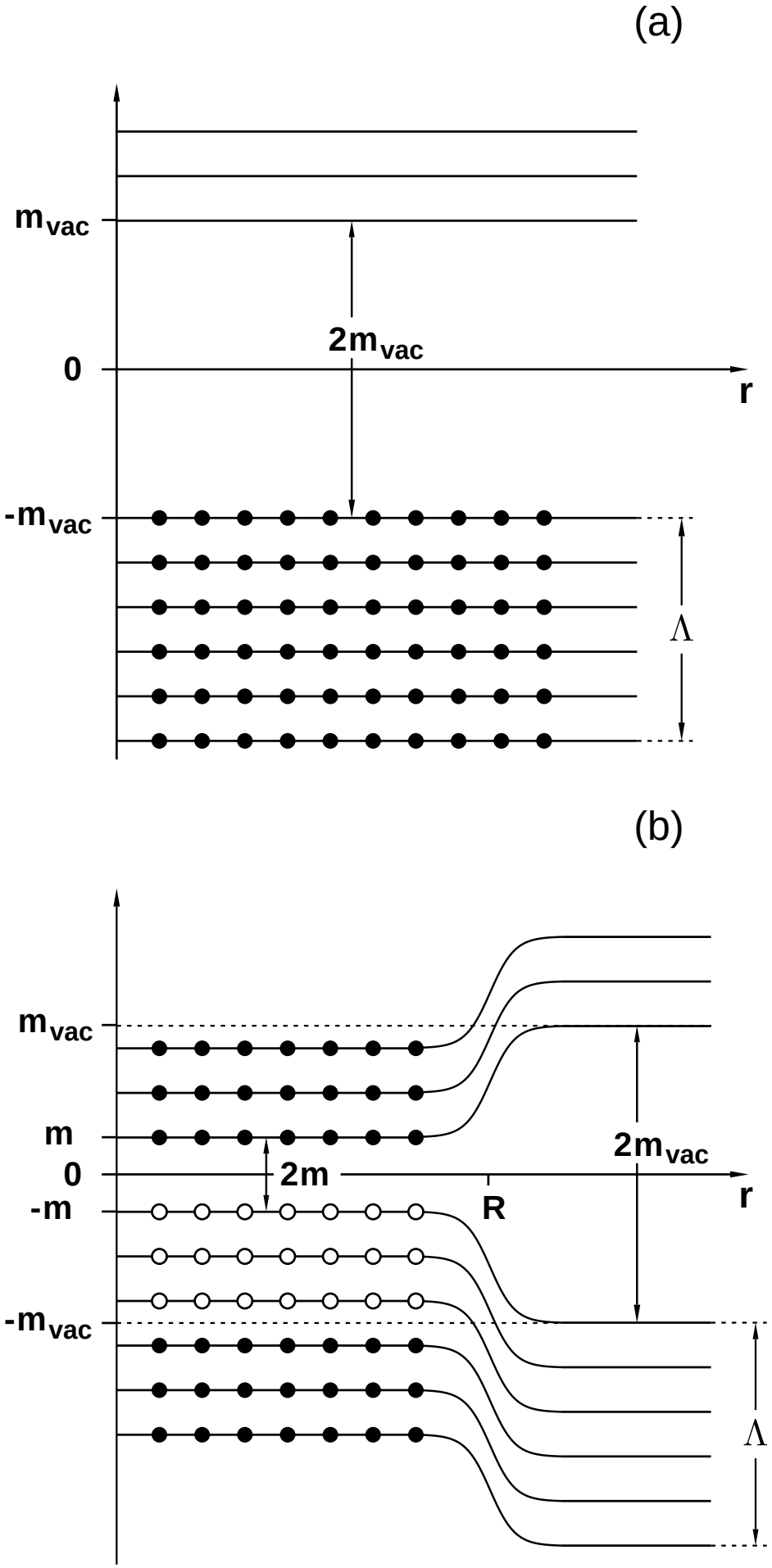

Fig. 1a,b

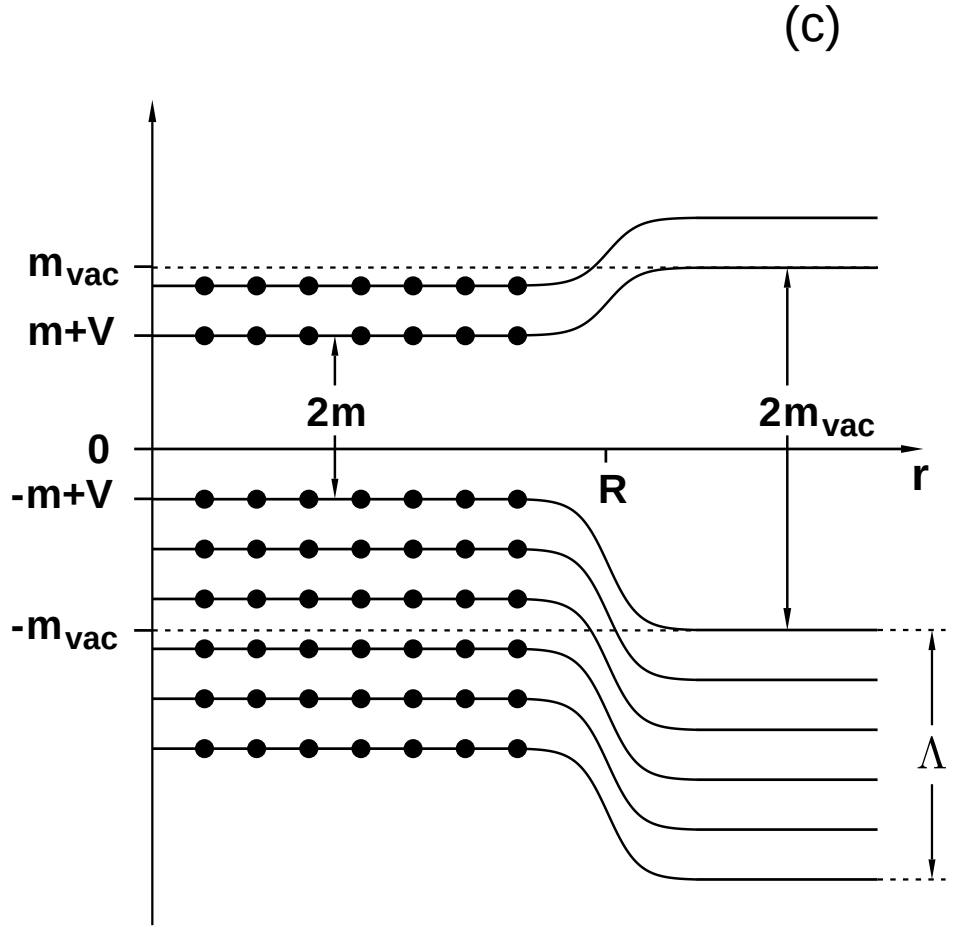

Fig. 1c

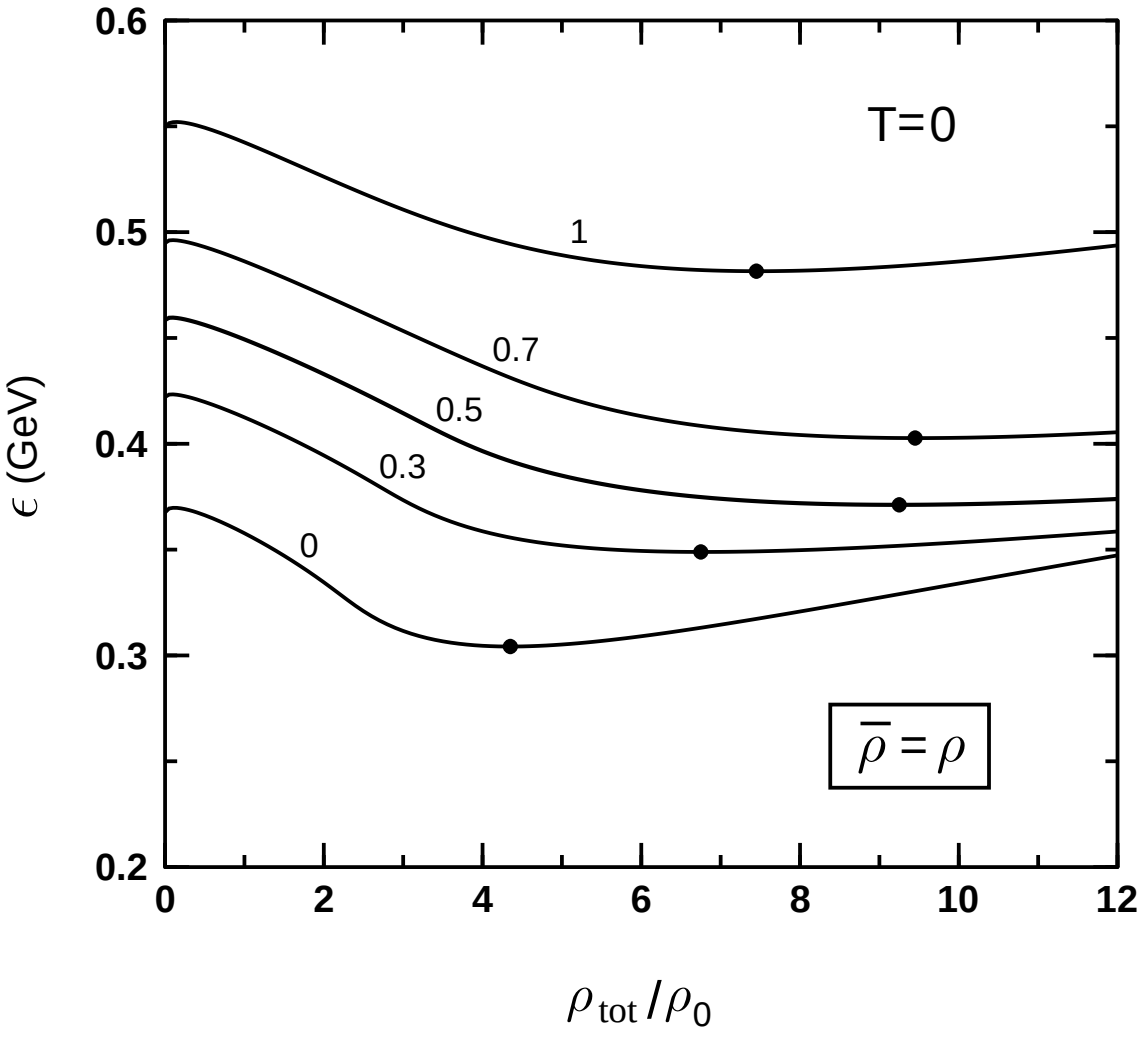
T=0
1
0.7
0.5
0.3
0
$\bar{\rho} = \rho$
ϵ (GeV)
ρ_{tot}/ρ_0
0.6
0.5
0.4
0.3
0.2
0
2
4
6
8
10
12

Fig. 2

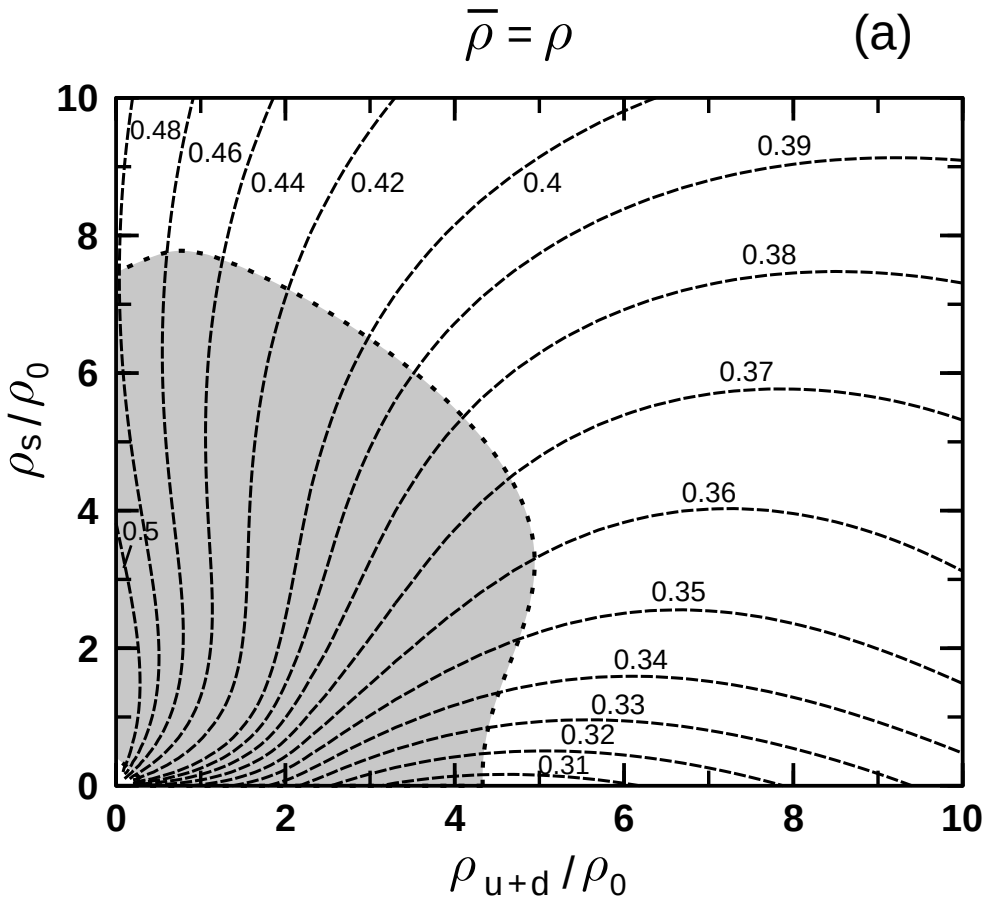
$\overline{\rho} = \rho$
(a)
0.48
0.46
0.44
0.42
0.4
0.39
0.38
0.37
0.36
0.35
0.34
0.33
0.32
0.31
0.5
ρ_s / ρ_0
ρ_{u+d} / ρ_0
0
2
4
6
8
10

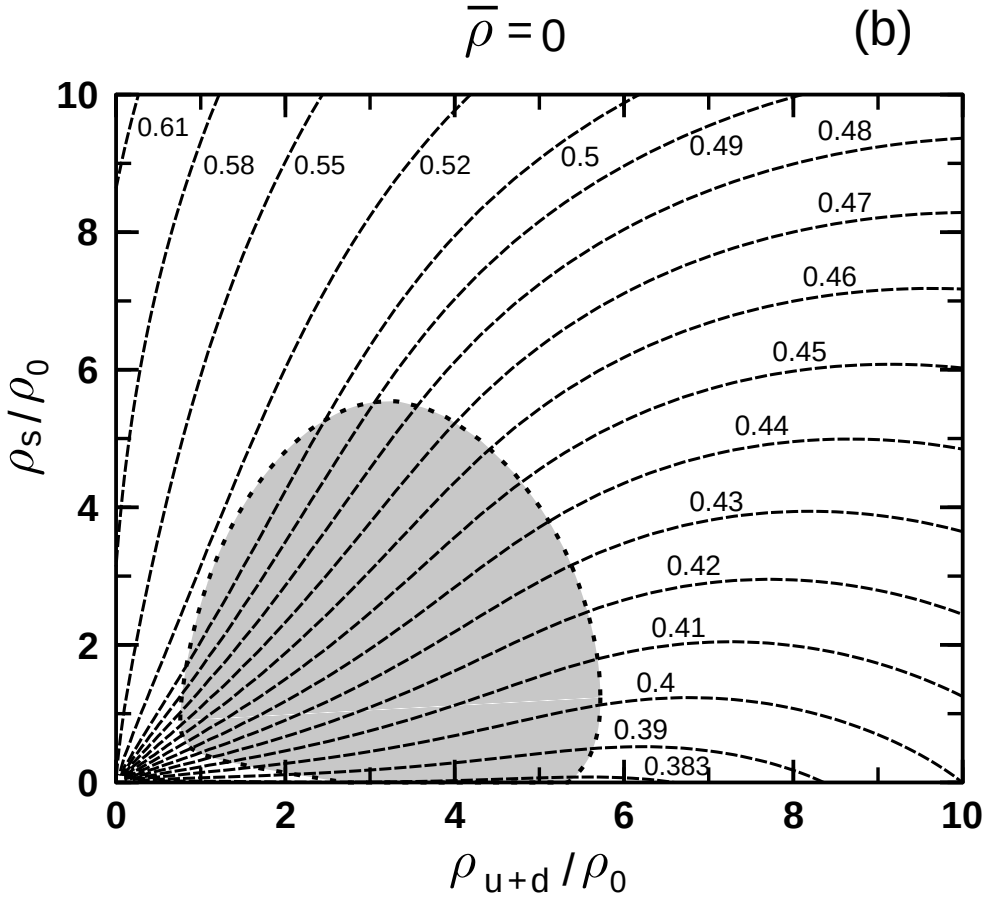
$\overline{\rho} = 0$
(b)
0.61
0.58
0.55
0.52
0.5
0.49
0.48
0.47
0.46
0.45
0.44
0.43
0.42
0.41
0.4
0.39
0.383
ρ_s / ρ_0
ρ_{u+d} / ρ_0
0
2
4
6
8
10

Fig. 3

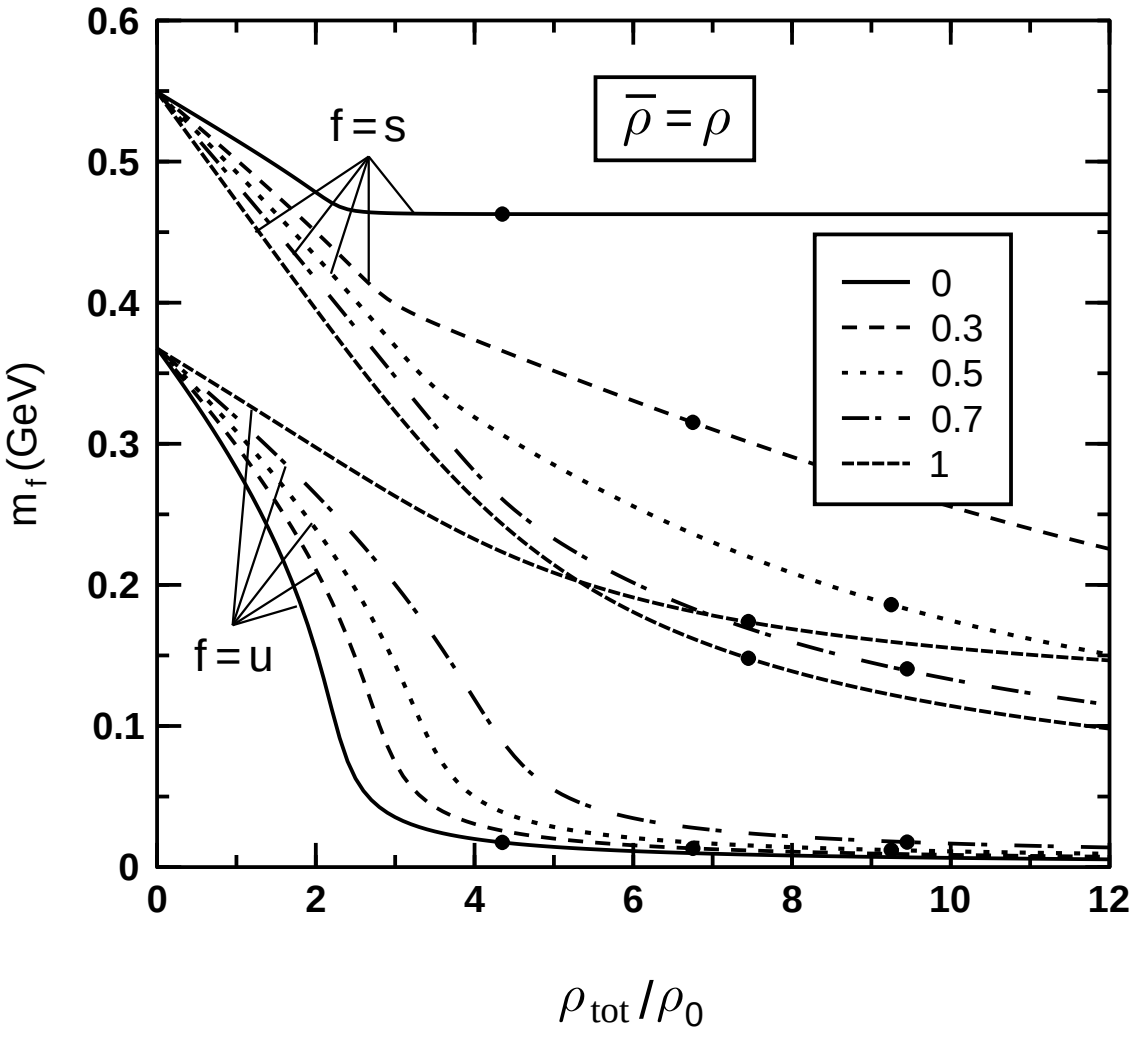
0.6
0.5
0.4
0.3
0.2
0.1
0
0
2
4
6
8
10
12
m_f (GeV)
ρ_{tot}/ρ_0
$\bar{\rho} = \rho$
f = s
f = u
0
0.3
0.5
0.7
1

Fig. 4

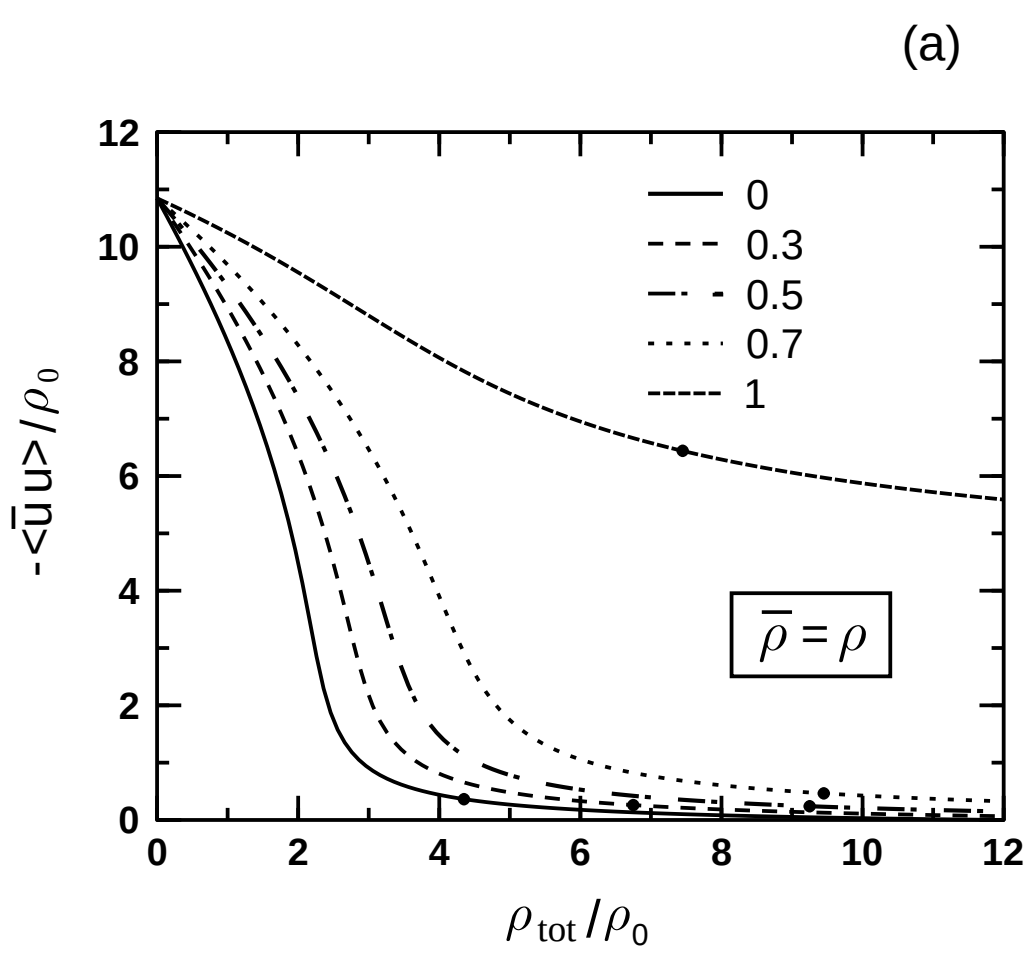
(a)
12
10
8
6
4
2
0
0
2
4
6
8
10
12
0
0.3
0.5
0.7
1
$\bar{\rho} = \rho$
$-\langle \bar{u} u \rangle / \rho_0$
$\rho_{\mathrm{tot}} / \rho_0$

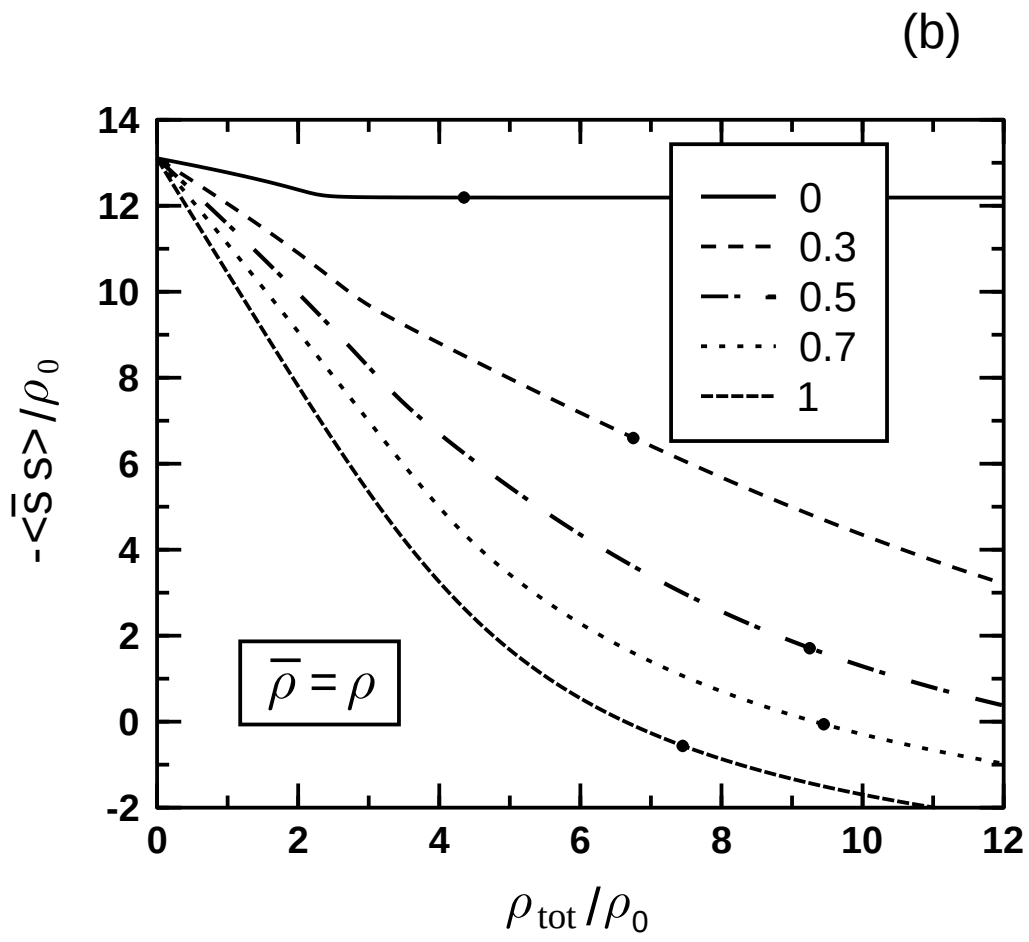
(b)
14
12
10
8
6
4
2
0
-2
0
2
4
6
8
10
12
0
0.3
0.5
0.7
1
$\bar{\rho} = \rho$
$-\langle \bar{s} s \rangle / \rho_0$
$\rho_{\mathrm{tot}} / \rho_0$

Fig. 5

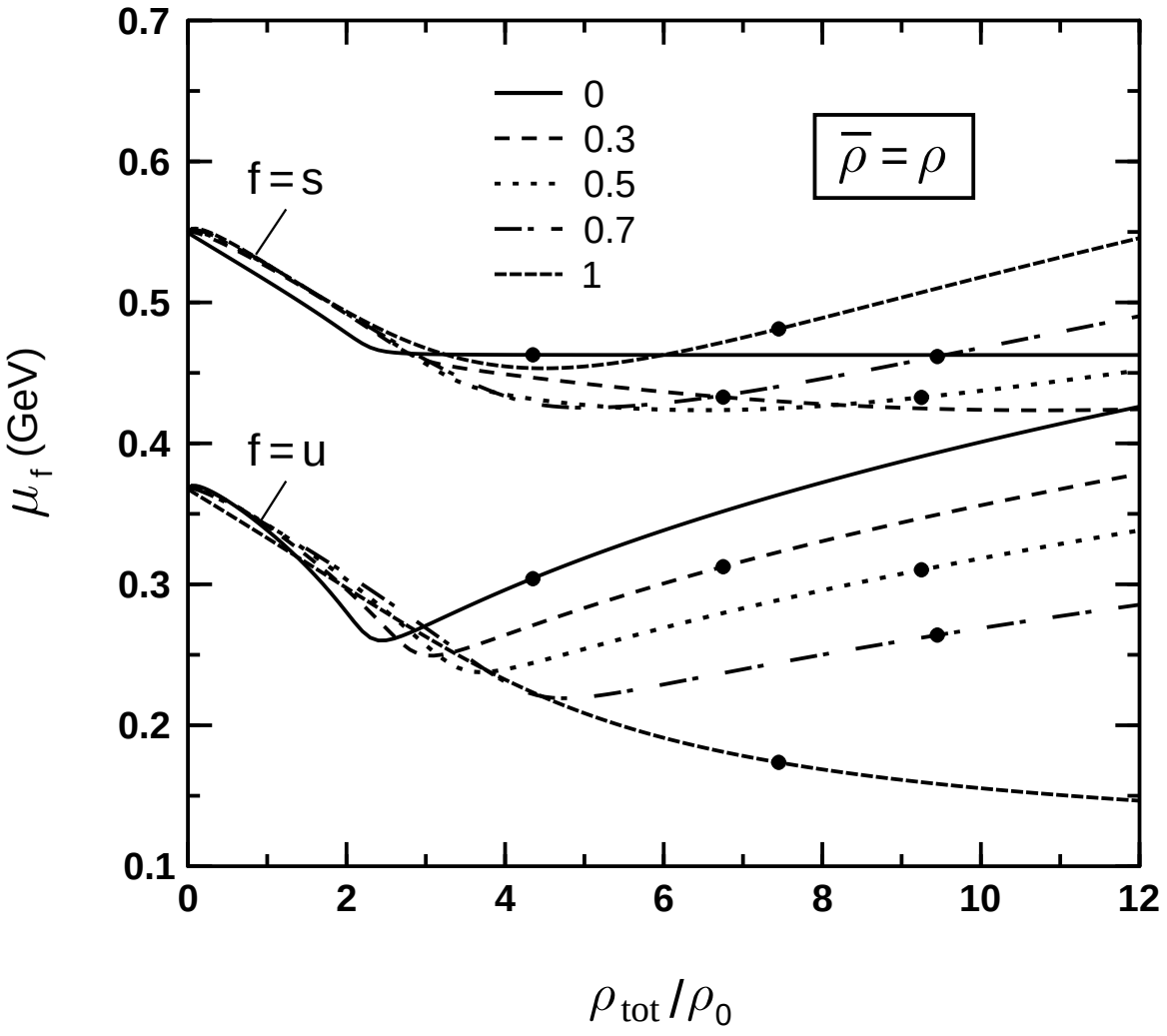
0.7
0.6
0.5
0.4
0.3
0.2
0.1
0
2
4
6
8
10
12
0
0.3
0.5
0.7
1
$\overline{\rho} = \rho$
f = s
f = u
μ_f (GeV)
ρ_{tot}/ρ_0

Fig. 6

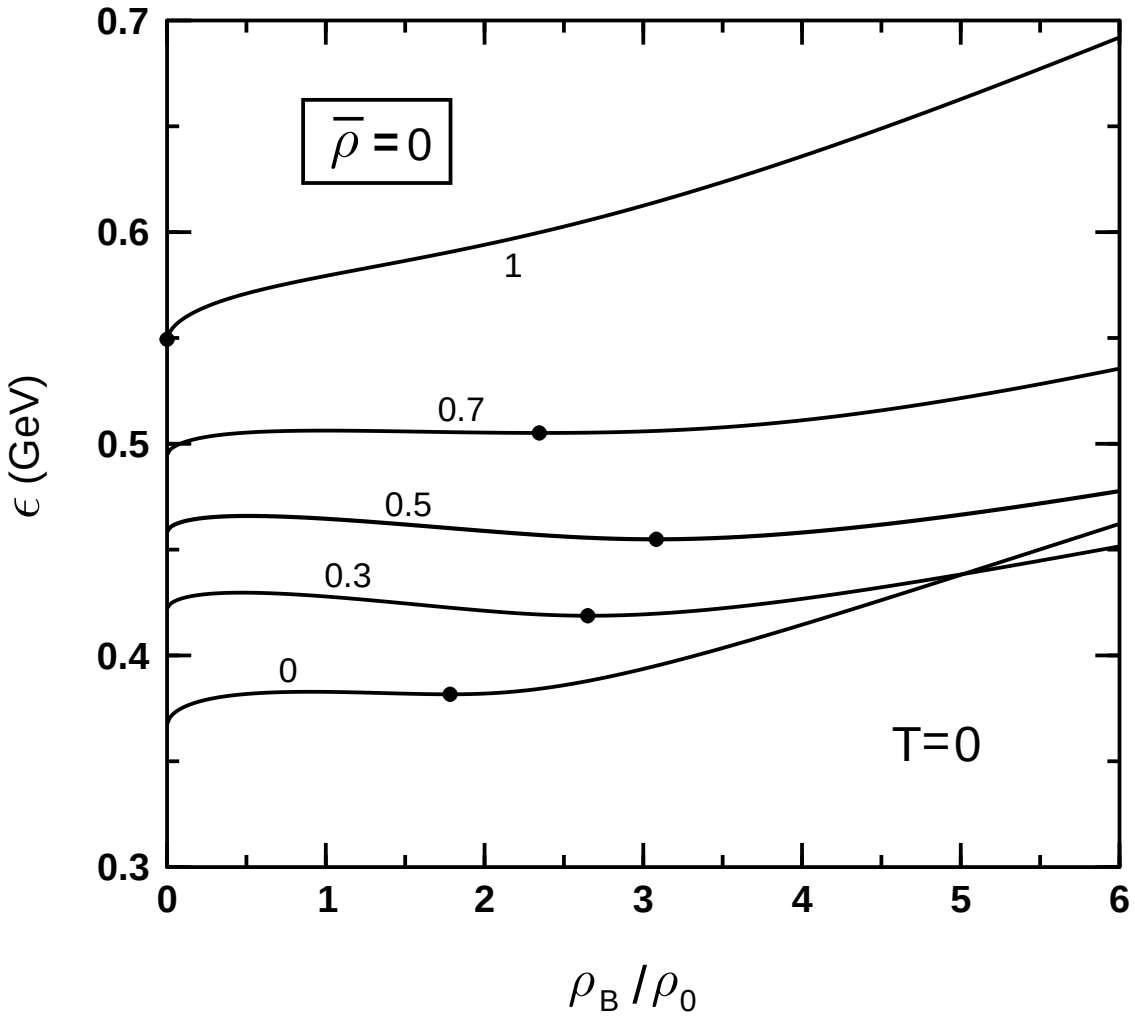
0.7
0.6
0.5
0.4
0.3
ϵ (GeV)
$\overline{\rho} = 0$
1
0.7
0.5
0.3
0
T=0
0
1
2
3
4
5
6
ρ_B / ρ_0

Fig. 7

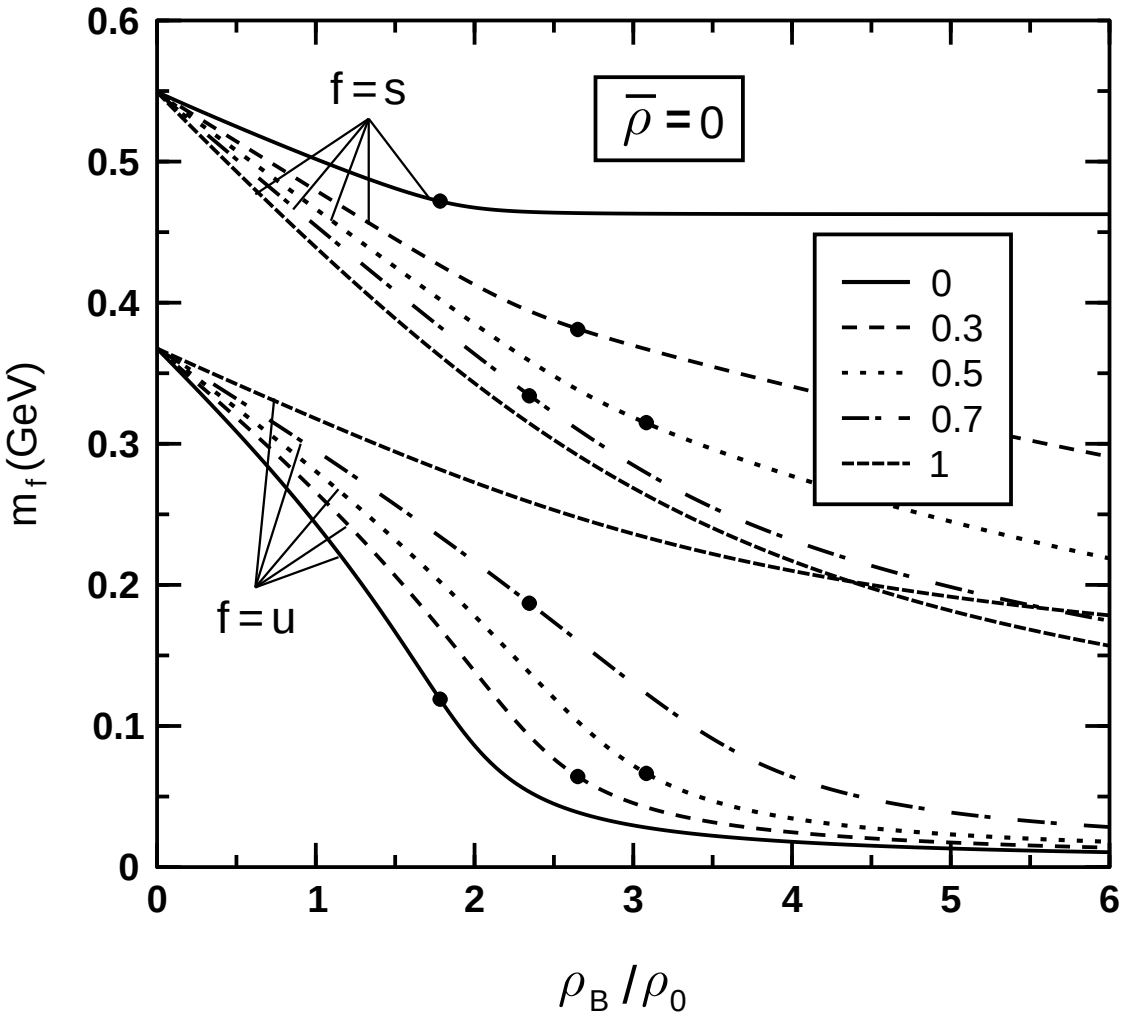
0.6
0.5
0.4
0.3
0.2
0.1
0
0
1
2
3
4
5
6
f = s
f = u
$\bar{\rho} = 0$
0
0.3
0.5
0.7
1
m_f (GeV)
ρ_B / ρ_0

Fig. 8

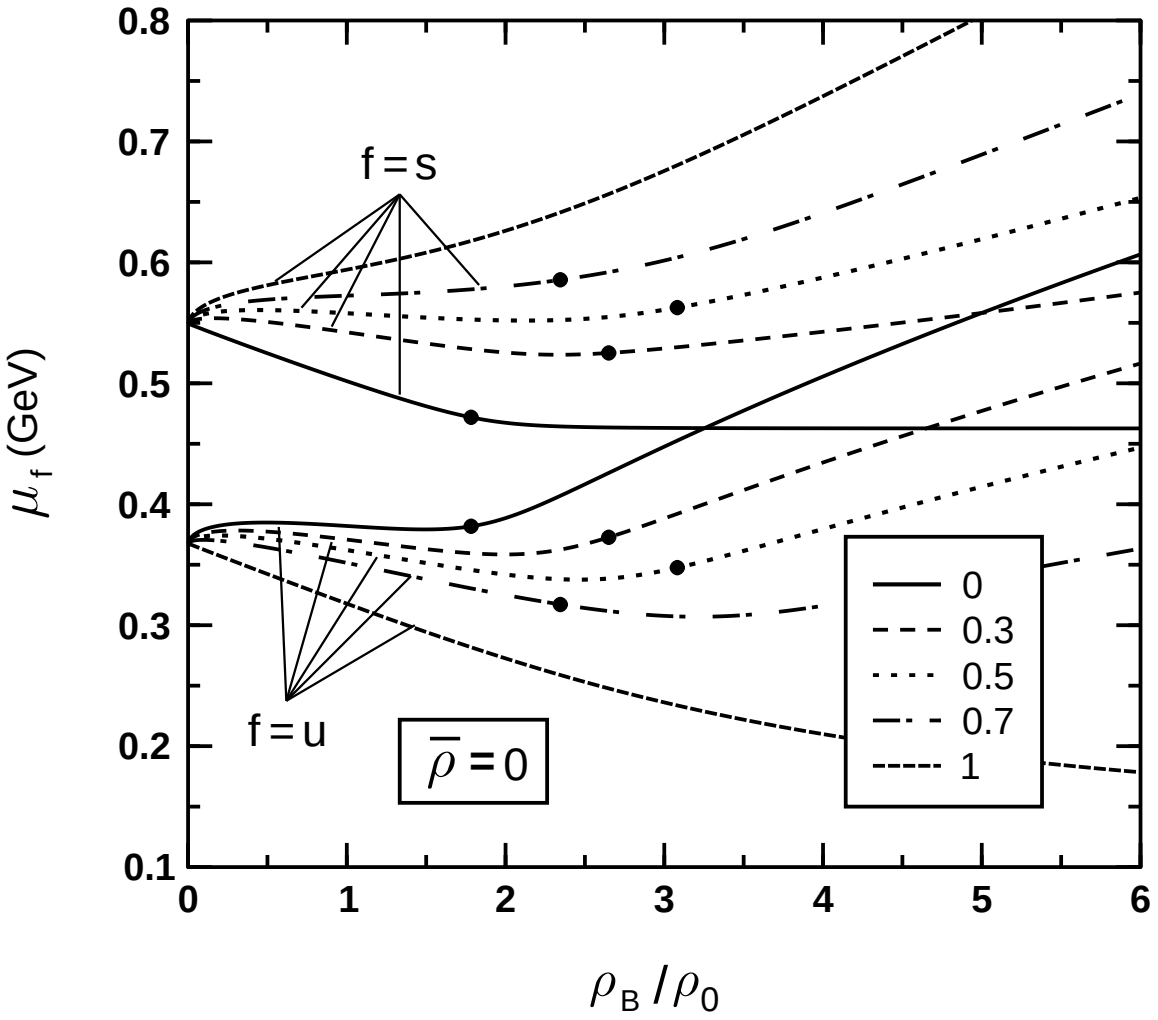
0.8
0.7
0.6
0.5
0.4
0.3
0.2
0.1
0
1
2
3
4
5
6
μ_f (GeV)
ρ_B / ρ_0
f = s
f = u
$\overline{\rho} = 0$
0
0.3
0.5
0.7
1

Fig. 9

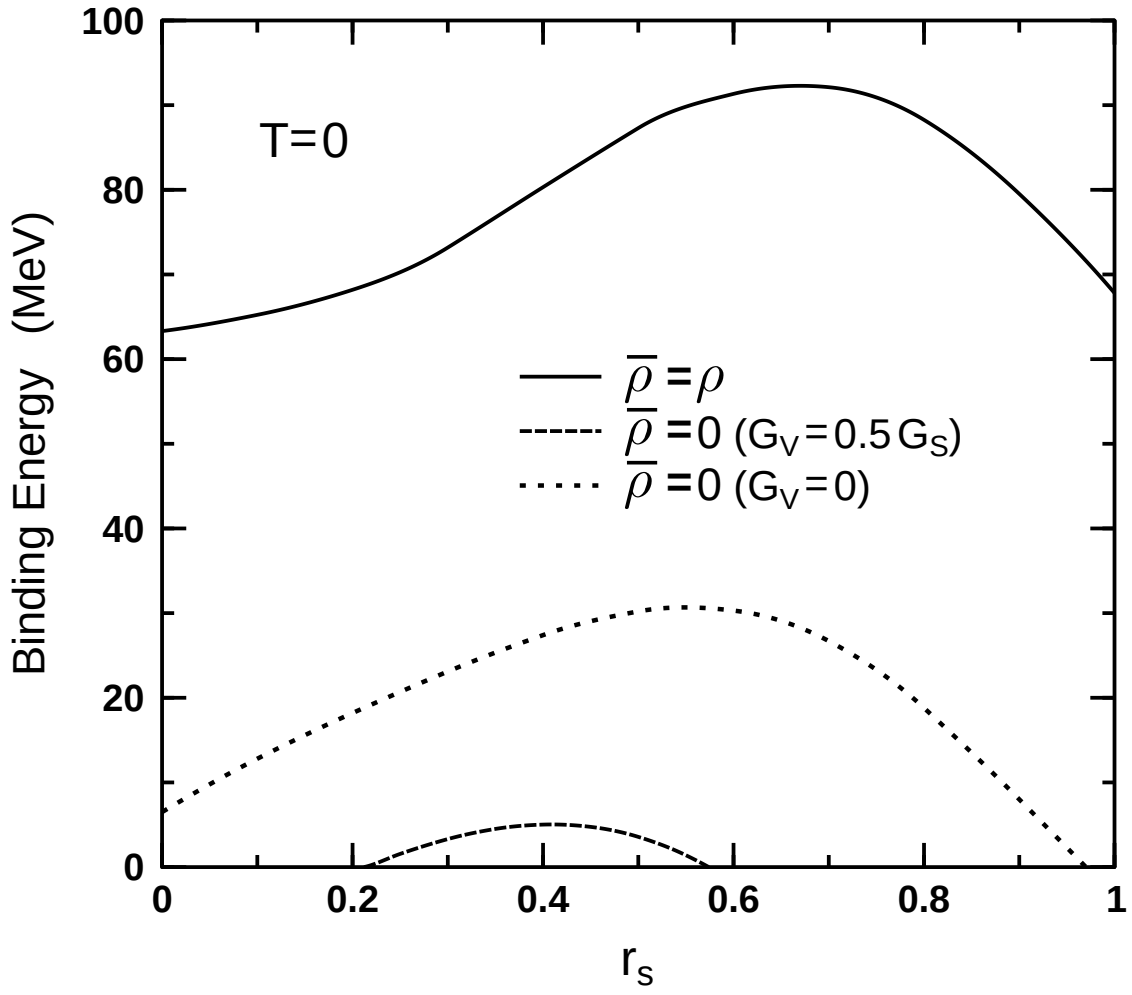
T=0
Binding Energy (MeV)
r_s
$\overline{\rho}=\rho$
$\overline{\rho}=0$ ($G_V=0.5\,G_S$)
$\overline{\rho}=0$ ($G_V=0$)
0
20
40
60
80
100
0
0.2
0.4
0.6
0.8
1

Fig. 10

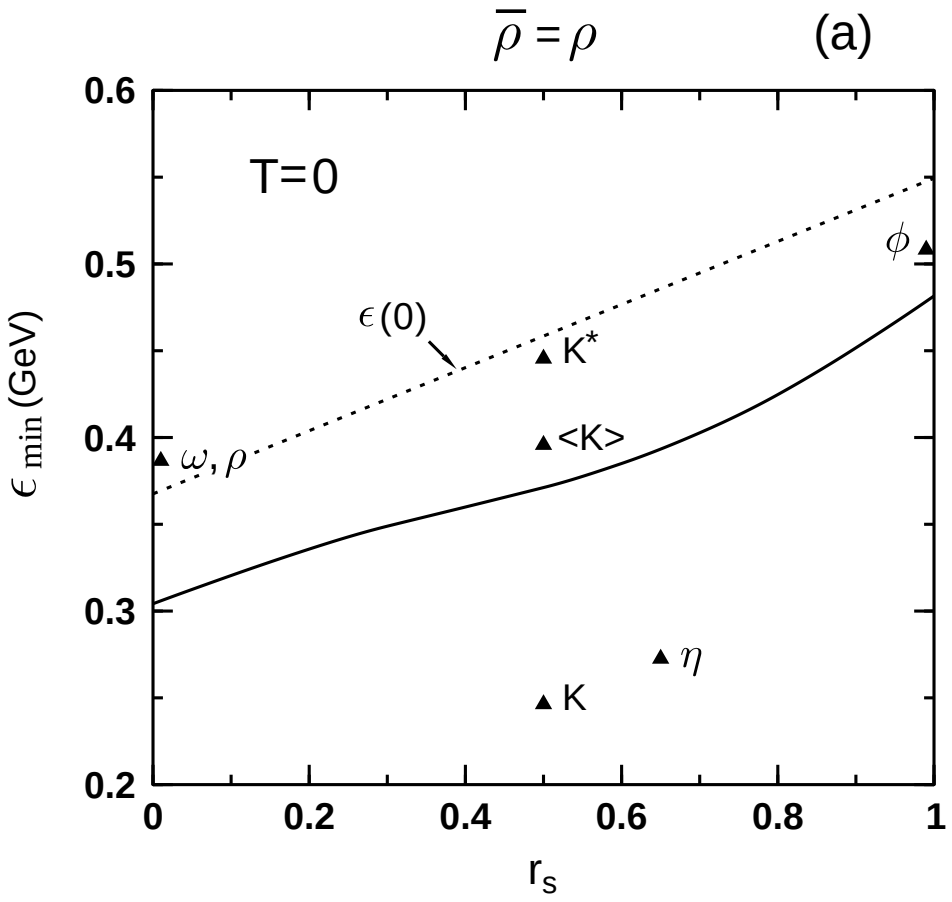
$\overline{\rho} = \rho$
(a)
T=0
$\epsilon(0)$
ϕ
K*
<K>
ω, ρ
η
K
ϵ_{min} (GeV)
r_s
0.2
0.3
0.4
0.5
0.6
0
0.2
0.4
0.6
0.8
1

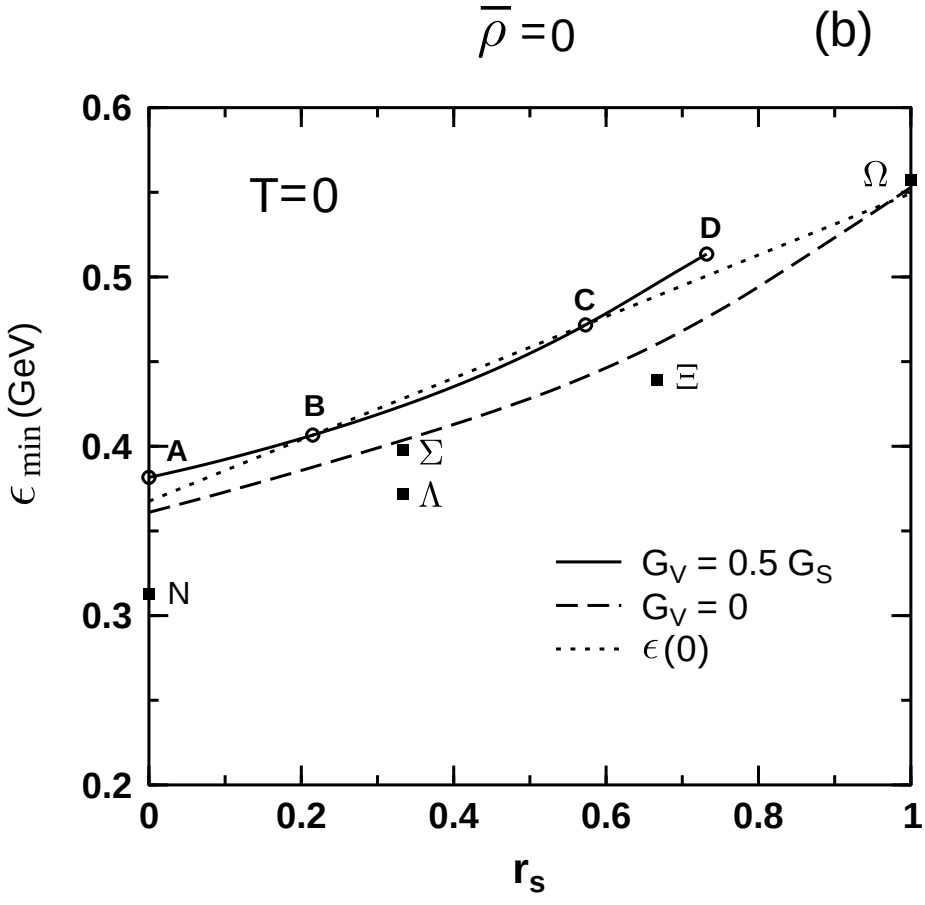
$\overline{\rho}$ =0
(b)
T=0
Ω
D
C
B
A
Ξ
Σ
Λ
N
$G_V = 0.5\ G_S$
$G_V = 0$
$\epsilon(0)$
ϵ_{min} (GeV)
r_s
0.2
0.3
0.4
0.5
0.6
0
0.2
0.4
0.6
0.8
1

Fig. 11

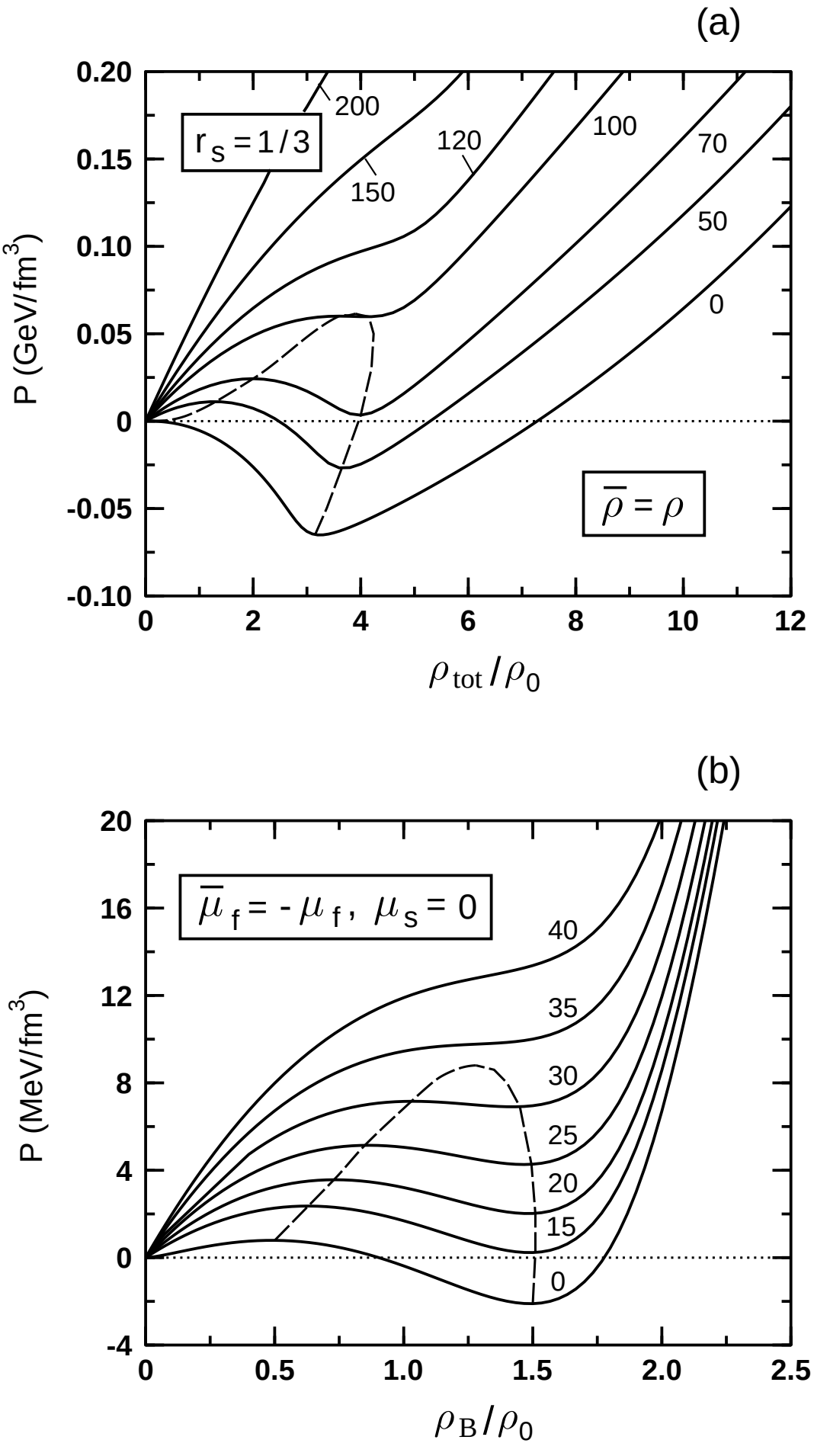
(a)
0.20
0.15
0.10
0.05
0
-0.05
-0.10
P (GeV/fm^3)
$r_s = 1/3$
200
150
120
100
70
50
0
$\bar{\rho} = \rho$
0
2
4
6
8
10
12
ρ_{tot}/ρ_0
(b)
20
16
12
8
4
0
-4
P (MeV/fm^3)
$\bar{\mu}_f = -\mu_f$, $\mu_s = 0$
40
35
30
25
20
15
0
0
0.5
1.0
1.5
2.0
2.5
ρ_B/ρ_0

Fig. 12

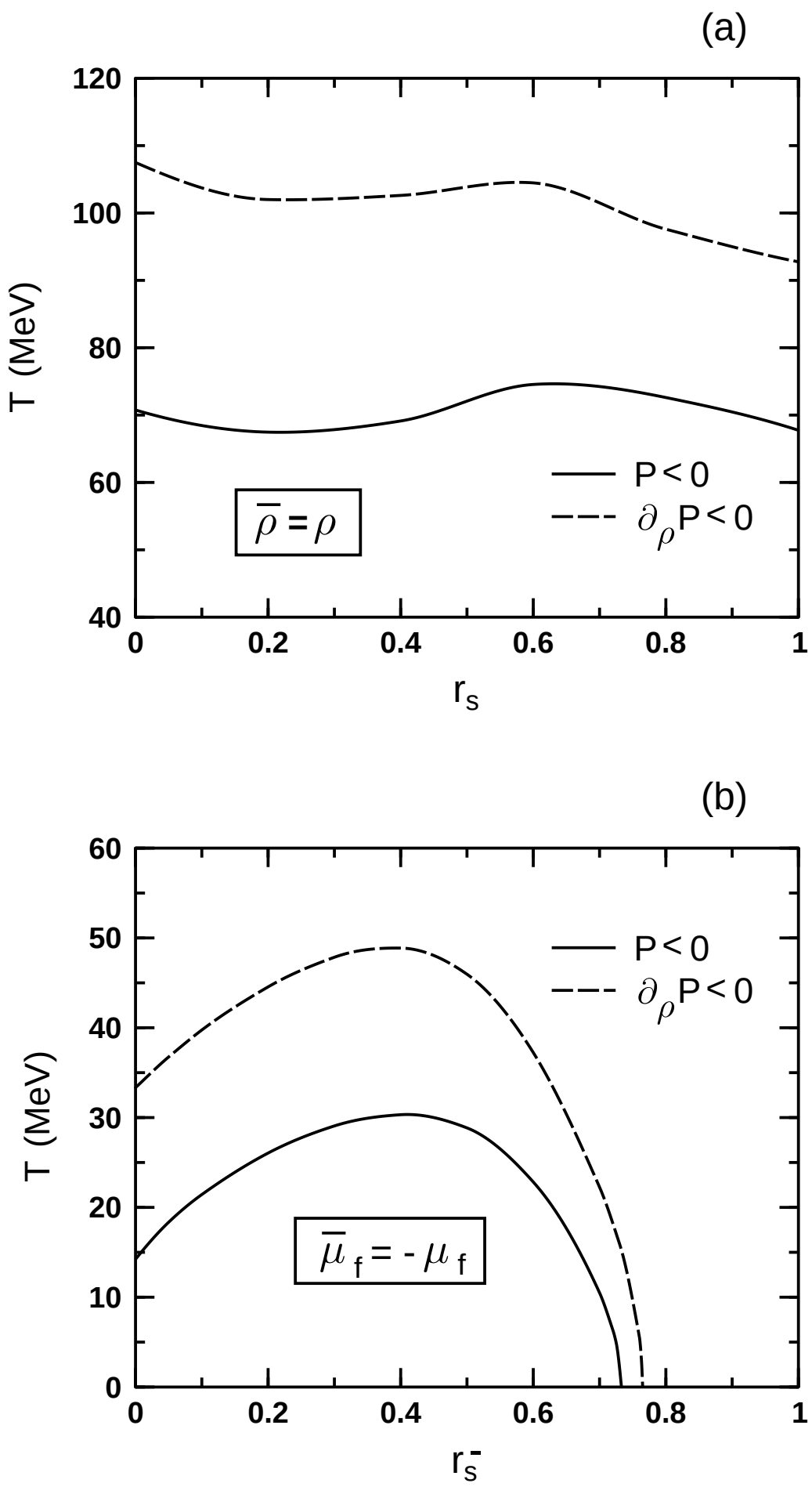
(a)
120
100
80
60
40
T (MeV)
0
0.2
0.4
0.6
0.8
1
r_s
P < 0
∂_ρP < 0
$\bar{\rho} = \rho$
(b)
60
50
40
30
20
10
0
T (MeV)
0
0.2
0.4
0.6
0.8
1
r_s
P < 0
∂_ρP < 0
$\bar{\mu}_f = -\mu_f$

Fig. 13

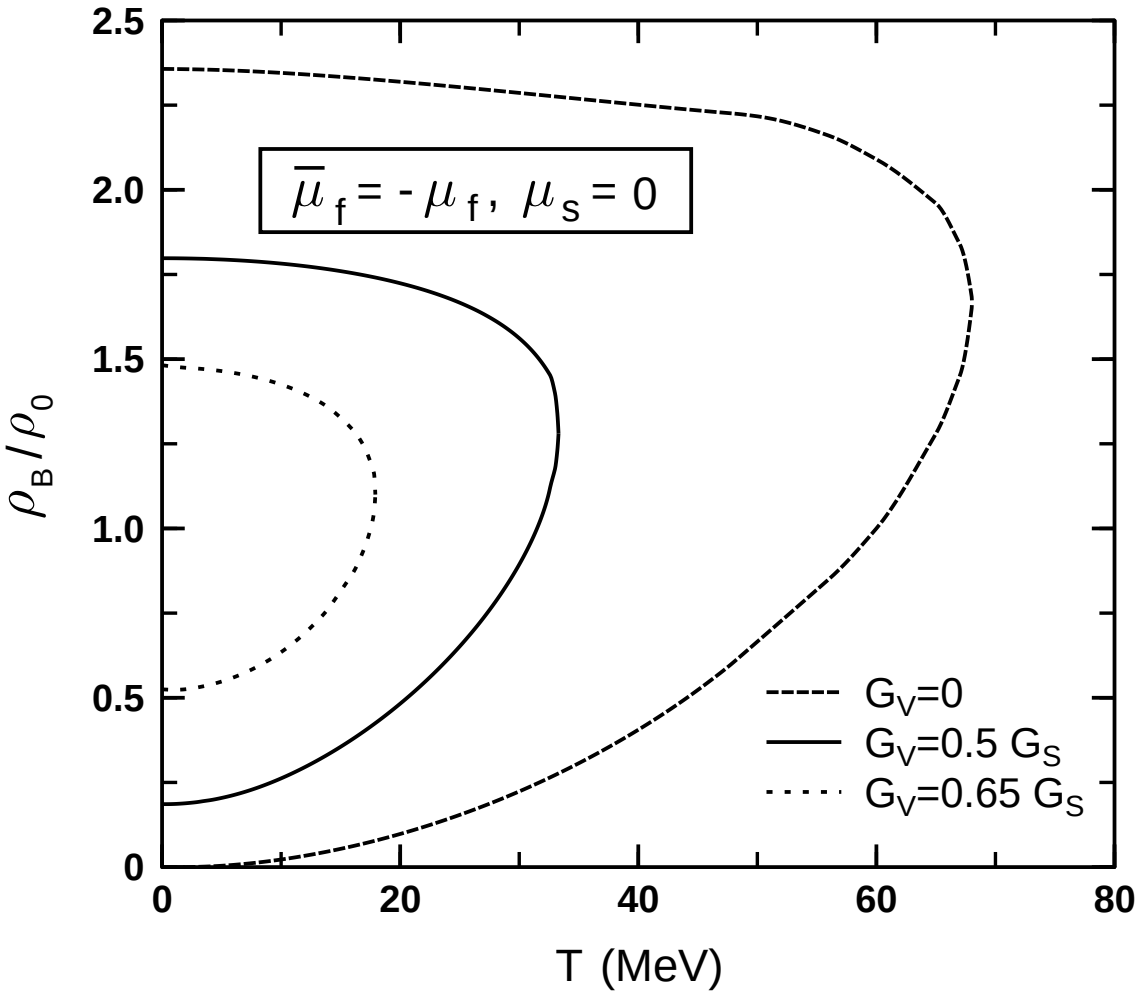
2.5
2.0
1.5
1.0
0.5
0
0
20
40
60
80
ρ_B/ρ_0
T (MeV)
$\bar{\mu}_f = -\mu_f,\ \mu_s = 0$
G_V=0
G_V=0.5 G_S
G_V=0.65 G_S

Fig. 14

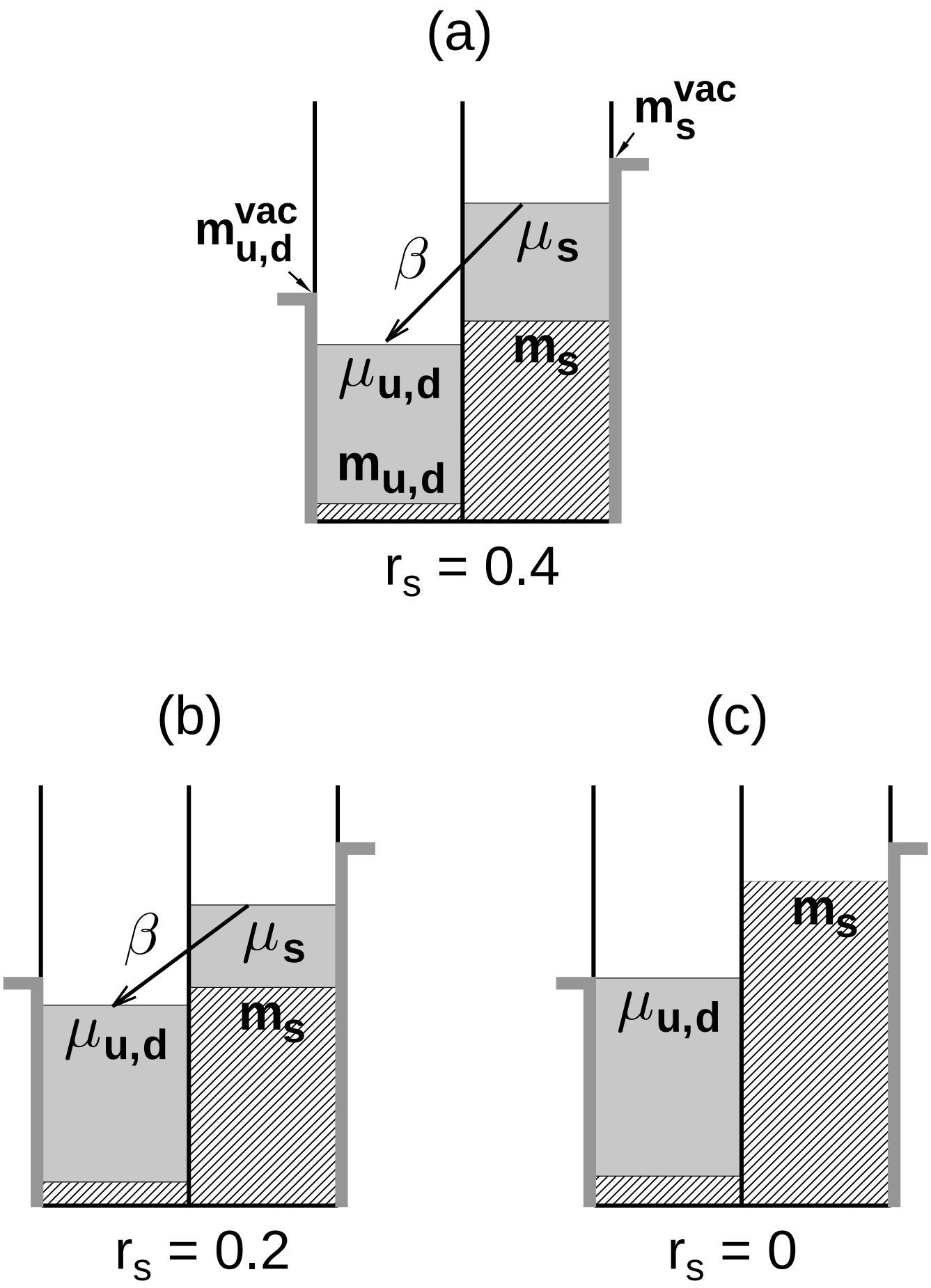
(a)
m_s^{vac}
$m_{u,d}^{vac}$
β
μ_s
m_s
$\mu_{u,d}$
$m_{u,d}$
$r_s = 0.4$
(b)
β
μ_s
m_s
$\mu_{u,d}$
$r_s = 0.2$
(c)
m_s
$\mu_{u,d}$
$r_s = 0$

Fig. 15